



HHS Public Access

Author manuscript

Annu Rev Biochem. Author manuscript; available in PMC 2016 September 21.

Published in final edited form as:

Annu Rev Biochem. 2013 ; 82: 497–530. doi:10.1146/annurev-biochem-052010-100934.

Methylerythritol Phosphate Pathway of Isoprenoid Biosynthesis

Lishan Zhao², Wei-chen Chang³, Youli Xiao¹, Hung-wen Liu³, and Pinghua Liu¹

Lishan Zhao: zhao@amyris.com; Wei-chen Chang: wchang1980@utexas.edu; Youli Xiao: ylxiao@bu.edu; Hung-wen Liu: h.w.liu@mail.utexas.edu; Pinghua Liu: pinghua@bu.edu

¹Department of Chemistry, Boston University, Boston, MA 02215

²Amyris, Inc., 5885 Hollis Street, Suite 100, Emeryville, CA 94608

³Division of Medicinal Chemistry, College of Pharmacy, and Department of Chemistry and Biochemistry, University of Texas at Austin, Austin, TX 78712

Abstract

Isoprenoids are a class of natural products with more than 50,000 members. All isoprenoids are constructed from two precursors, isopentenyl diphosphate (IPP) and its isomer dimethylallyl diphosphate (DMAPP). Two of the most important discoveries in isoprenoid biosynthetic studies in recent years are the elucidation of a second isoprenoid biosynthetic pathway (the methylerythritol phosphate (MEP) pathway) and a modified mevalonate (MVA) pathway. In this review, mechanistic insights on the MEP pathway enzymes are summarized. Since many isoprenoids have important biological activities, the need to produce them in sufficient quantities for downstream research efforts or commercial application is apparent. Recent advances in both the MVA and MEP pathway-based synthetic biology efforts are also illustrated by reviewing the landmark work of artemisinic acid and taxadien-5 α -ol production through microbial fermentations.

Keywords

Isoprenoids; biosynthesis; enzyme mechanism; metabolic engineering; synthetic biology; methylerythritol phosphate (MEP) pathway; mevalonate (MVA) pathway

I. INTRODUCTION

In the literature, "isoprenoid", "terpenoid", and "terpene" are used interchangeably to refer to a class of natural products built from two isoprene units, isopentenyl diphosphate (IPP, **1**, Figure 1) and dimethylallyl diphosphate (DMAPP, **2**). As one of the largest and structurally most diverse groups of natural products with more than 55,000 members (1), isoprenoids play key metabolic, structural, and regulatory roles in all kingdoms of life. In addition, many monoterpenes, sesquiterpenes, and diterpenes produced as secondary metabolites are pheromones or defensive agents and are involved in many aspects of our life, including medicine (2, 3), flavor and fragrances (4), and nutrition (5). For decades, the mevalonic acid (MVA, **6**) pathway was thought to be the only IPP and DMAPP biosynthetic pathway (6, 7). However, the incompatibility of many isotopic labeling results with the MVA paradigm had long been puzzling. Efforts to resolve such discrepancies eventually led to the discovery of the 2-*C*-methyl-D-erythritol 4-phosphate (MEP, **13**) pathway, also known as the 1-deoxy-D-

xylulose 5-phosphate (DXP, **12**) or non-mevalonate pathway (Figure 1C) (8–10). Since many human pathogens rely exclusively on the MEP pathway for the biosynthesis of their isoprenoid compounds, a study of the enzymes on this pathway with an ultimate goal of developing inhibitors as potential drugs has been a subject pursued by many groups (11–16). In addition to their therapeutic value, mechanistic investigation of the MEP pathway enzymes has also attracted significant attention as many of them catalyze unusual chemical transformations whose mechanisms remain obscure. In this review, we will summarize the recent progress in our understanding of the MEP pathway, focusing on the catalytic mechanisms of the enzymes involved. Despite the high demand of many isoprenoids for chemical and biomedical applications, their production, either from the natural sources or through chemical synthesis, remains a challenging task. Thus, exploiting the isoprenoid biosynthetic machineries offers a promising approach for acquiring target isoprenoids and the creation of analogues not easily obtainable by synthetic means. This review will also highlight some recent achievements on microbial-based isoprenoid production.

II. BIOSYNTHESIS OF ISOPRENOID PRECURSORS (IPP AND DMAPP)

For decades, the MVA pathway (Figure 1A) was thought to be the only pathway for the biosynthesis of IPP (**1**) and DMAPP (**2**) (6, 7). This pathway starts with the condensation of two molecules of acetyl-CoA (**3**) to form acetoacetyl-CoA (**4**). Further condensation with a third molecule of acetyl-CoA produces 3-hydroxy-3-methyl-glutaryl-CoA (HMG-CoA, **5**), which is then reduced by HMG-CoA reductase (HMGR) to give MVA (**6**). Following two consecutive phosphorylation steps catalyzed by mevalonic acid kinase (MVK) and phosphomevalonate kinase (PMK), the resulting mevalonate-5-diphosphate (**8**) is converted to IPP (**1**) in an ATP-coupled decarboxylation reaction catalyzed by mevalonate-5-diphosphate decarboxylase (MPD). An IPP:DMAPP isomerase (IDI) is responsible for the interconversion between IPP (**1**) and DMAPP (**2**). Recently, Grochowski *et al.* (17) identified an enzyme from *Methanocaldococcus jannaschii* capable of phosphorylating isopentenyl phosphate (**9**) to IPP (**1**). A modified MVA pathway was thus proposed (Figure 1B), in which mevalonate-5-phosphate (**7**) is decarboxylated to **9** and then phosphorylated by isopentenyl phosphate kinase (IPK) to form IPP (**1**) (18–20). However, the proposed phosphomevalonate decarboxylase (PMD, **7** → **9** conversion) has yet to be identified.

The MEP pathway (Figure 1C) was discovered in the 1990s (21, 22). The history of this remarkable discovery has been covered in a few reviews (8–10). This pathway is initiated with a thiamin diphosphate-dependent condensation between D-glyceraldehyde 3-phosphate (**11**) and pyruvate (**10**) to produce DXP (**12**), which is then reductively isomerized to MEP (**13**) by DXP reducto-isomerase (DXR/IspC). Subsequent coupling between MEP (**13**) and cytidine 5'-triphosphate (CTP) is catalyzed by CDP-ME synthetase (IspD) and produces methylerythritol cytidyl diphosphate (CDP-ME, **14**). An ATP-dependent enzyme (IspE) phosphorylates the C₂ hydroxyl group of **14**, and the resulting 4-diphosphocytidyl-2-C-methyl-D-erythritol-2-phosphate (CDP-MEP, **15**) is cyclized by IspF to 2-C-methyl-D-erythritol-2,4-cyclodiphosphate (MEcPP, **16**). IspG catalyzes the ring-opening of the cyclic pyrophosphate and the C₃-reductive dehydration of MEcPP (**16**) to 4-hydroxy-3-methylbutenyl 1-diphosphate (HMBPP, **17**). The final step of the MEP pathway is catalyzed by

IspH and converts **17** to both IPP (**1**) and DMAPP (**2**). Thus, unlike the MVA pathway, IPP:DMAPP isomerase (IDI) is not essential in many MEP pathway utilizing organisms.

Clearly, the MVA and MEP pathways represent two different strategies employed by Nature to synthesize the five-carbon isoprene units. In addition, there is a well-defined distribution between the MVA and MEP pathways among different kingdoms (8). The MEP pathway has been identified in eubacteria, green algae, and higher plants, whereas the MVA pathway is found in animals, plants (cytosol), fungi, and archaea. Plants are unique in that they have both MEP and MVA pathways, albeit with a compartmental segregation between them. It was thus proposed that the MEP pathway enzymes could be excellent targets for developing new broad-spectrum antibiotics and herbicides. This subject has been extensively discussed in many excellent recent reviews (11–16). In the following section, we will summarize mechanistic studies on the MEP pathway enzymes, especially the transformations catalyzed by IspG (**16** → **17**) and IspH (**17** → **1/2**), which are mechanistically intriguing.

III. MECHANISTIC STUDIES OF THE MEP PATHWAY ENZYMES

III.1. 1-Deoxy-D-xylulose 5-phosphate synthase (DXS)

DXS is a thiamine diphosphate (TPP) dependent-enzyme and exhibits weak sequence homology (~20% identity) to transketolase and the E1 subunit of pyruvate dehydrogenase (23, 24). It is a homo-dimeric protein (25) that catalyzes the condensation between pyruvate (**10**) and D-glyceraldehyde 3-phosphate (**11**) to generate DXP (**12**), which is also a precursor for vitamins B₁ (26) and B₆ (27). The DXS-catalyzed reaction, as depicted in Figure 2A, starts with TPP cofactor activation. Coupling of the resulting ylide (**18**) with pyruvate (**10**) followed by decarboxylation affords a carbanion/enamine intermediate (**19**). Subsequent nucleophilic attack of the second substrate (**11**) by intermediate **19**, followed by the elimination of DXP (**12**) completes the catalytic cycle. Kinetically, the DXS-catalyzed reaction follows a sequential mechanism with pyruvate (**10**) as the first substrate (28). In the absence of **11**, DXS can catalyze the condensation between two molecules of pyruvate (**10**) to produce acetolactate.

III.2. 1-Deoxy-D-xylulose 5-phosphate reductoisomerase (DXR)

DXR catalyzes a reversible intramolecular rearrangement reaction between DXP (**12**) and MEP (**13**), with the equilibrium favoring MEP (Figure 1C) (29). Both NADPH and a divalent cation are required for catalysis (30, 31). DXR has been extensively studied as a promising target for new antimicrobial therapy (15). Current biochemical data suggest that DXR catalysis might follow a retro-aldol/aldol mechanistic model (Figure 2B) (30). In this model, DXP first fragments in a retro-aldol manner between C₃-C₄ to generate a three carbon (hydroxyacetone, **21**) and a two-carbon phosphate intermediate (**22**), which are then reunited by C-C bond formation through an aldol reaction to form methylerythrose-5-phosphate (**20**). NADPH reduces **20** stereo-specifically to produce MEP (**13**). The step of **20** → **13** conversion by NADPH reduction was ruled out as the rate-limiting step in a pre-steady state kinetic isotope effect study, suggesting that one of the steps leading to intermediate **20** (Figure 2B) might be rate limiting (32). Such a hypothesis was supported by results from kinetic isotopic studies using both [3-²H]-DXP and [4-²H]-DXP. For the retro-

aldol/aldol model, both C₃ and C₄ undergo sp³ to sp² rehybridization in the fragmentation step. Therefore, both [3-²H]-DXP and [4-²H]-DXP should display secondary kinetic isotopic effects if the DXP fragmentation is part of the rate-limiting step. Results from studies using [3-²H]-DXP and [4-²H]-DXP showed normal secondary kinetic isotopic effect (1.04 ± 0.02 and 1.11 ± 0.02), and are consistent with the retro-aldol/aldol mechanism (33, 34). While the natural substrate for DXR is (3*S*, 4*R*)-DXP (**12**), the enzyme has also been reported to catalyze the production of (3*S*, 4*S*)-DXP (**23**) from (3*S*, 4*R*)-DXP (**12**) in the absence of divalent cation and NADPH. However, this reaction occurs at a rate that is orders of magnitude slower than the normal catalytic turnover rate (33). The formation of **23** was also observed in one of the reported crystal structures (35). These results were interpreted as additional lines of evidence supporting the retro-aldol/aldol model. The DXR-catalyzed reaction has been explored using various substrate analogs (32, 36–39) and results from these studies are also consistent with the retro-aldol/aldol condensation model.

III.3. Formation of MEcPP from MEP by IspD, IspE, and IspF-catalyzed reactions

IspD, IspE, and IspF catalyze the activation of MEP (**13**) and the subsequent cyclization to form MEcPP (**16**, Figure 1C). Biochemical characterizations, inhibitor development, and structural studies of these three enzymes have been discussed in detail in recent reviews (14, 15). However, some unique features of these enzymes are summarized here. Besides catalyzing the physiological reaction (**15** → **16**), *E. coli* and *Plasmodium falciparum* IspF can also catalyze the conversion of CDP-ME (**14**) to 2C-methyl-D-erythritol 3,4-cyclophosphate (**24**) (Figure 2C) (40, 41). However, the rate of this reaction is only ~1% of the physiological reaction (**15** → **16**). The malaria recombinant IspF also catalyzes the formation of 2-phospho-2C-methyl-D-erythritol 3,4-cyclophosphate (**25**) from CDP-MEP (**15**) with a rate that is ~10% of the **15** → **16** conversion (41). Interestingly, IspDF bifunctional proteins have been found in many organisms (42–44). This type of fusion is unique in that the parent monofunctional enzymes (IspD and IspF) catalyze two non-consecutive steps in the MEP pathway (Figure 1C).

III.4. 2-C-methyl-D-erythritol-2,4-cyclodiphosphate reductase (IspG)

Our knowledge on IspG catalysis, an iron-sulfur cluster containing protein mediated reductive dehydration reaction, lags far behind that on the earlier enzymes in the MEP pathway. Thus, IspG studies over the last decade will be summarized in three directions: 1) Characterizing the IspG iron-sulfur cluster; 2) Improving the *in vitro* IspG activity; and 3) Mechanistic studies on IspG.

III.4.1. Characterizing the IspG iron-sulfur cluster—IspG catalyzes the ring opening of the cyclic pyrophosphate and C₃-reductive dehydration of MEcPP (**16**) to HMBPP (**17**) (45–50). Holo-IspG (51, 52) can be obtained by co-expression with an iron-sulfur cluster maturation system (e.g., *isc* operon) (53). *In vivo* iron-sulfur cluster assembly might also require a specific scaffold protein, ErpA (54). *In vitro*, the iron-sulfur cluster can be installed by the reconstitution of apo-IspG using FeCl₃ and Na₂S under reducing conditions (55, 56). Mössbauer characterization of the [⁵⁷Fe] reconstituted IspG indicates the presence of a [4Fe-4S]²⁺ cluster with one of its iron sites coordinated by a non-cysteine ligand (56). This has been confirmed by the recently reported crystal structures of *Aquifex aeolicus* (57) and

Thermus thermophilus IspGs (58) (Figure 3A). The [4Fe-4S] cluster is at the C-terminal end of IspG and is coordinated by Cys265, Cys268, Cys300, and Glu307 (*A. aeolicus* IspG). The recruitment of a Glu residue as an iron-sulfur cluster ligand is unique in iron-sulfur containing proteins (59, 60). IspG is a homodimer and the two subunits interact with each other in a head-to-tail fashion (Figure 3A). Each subunit has two domains: the N-terminal TIM-barrel domain (residues 1 – 254 of *A. aeolicus* IspG) that has the proposed MEcPP binding site; and the iron-sulfur cluster containing C-terminal $\alpha\beta$ domain (residues downstream from 259 of *A. aeolicus* IspG). Within one subunit, the proposed MEcPP binding site and the [4Fe-4S] cluster are too far from each other (~56 Å, Figure 3A). It was thus suggested that the active site is located at the subunit interface, formed between the N-terminal domain of one subunit and the C-terminal domain of the other subunit (Figure 3A) (57, 58). Results from biochemical and spectroscopic characterizations (section III.4.3) suggest that MEcPP interacts directly with the [4Fe-4S] cluster. Because the proposed MEcPP binding site is still ~20 Å away from its adjacent [4Fe-4S] cluster on the other subunit (Figure 3A), it raises the possibility of an MEcPP binding triggered conformation change to bring the proposed MEcPP binding site and the [4Fe-4S] cluster in close proximity for catalysis. To date, a crystal structure of the MEcPP-IspG complex is not yet available. The MEcPP binding site shown in Figure 3A is proposed based on bioinformatic analysis and site-directed mutagenesis studies. The validity of this model and the MEcPP activation mechanism remain to be established.

III.4.2. Improving the *in vitro* IspG activity—The correct installation of the IspG [4Fe-4S] cluster is essential for IspG functionality (section III.4.1). Since IspG-catalysis is a reductive dehydration reaction (Figure 1C), using a proper reduction system to reduce its [4Fe-4S]²⁺ to a [4Fe-4S]¹⁺ is another key factor that governs IspG activity. Puan *et al.* proposed that flavodoxin I is the *in vivo* reduction system for *E. coli* IspG (61). Since flavodoxins are absent in the plant plastids and the apicomplexa plastid-like organelle, Seemann *et al.* demonstrated that ferredoxin could support *Arabidopsis* IspG catalysis (62). Studies using bacterial two-hybrid system and direct pull-down assays indicated that cyanobacteria IspG also interact with ferredoxin (63). However, results from *in vitro* studies suggest that other factors might also be required (52, 64). For example, when the NADPH-flavodoxin/flavodoxin reductase system was used to reduce *E. coli* IspG, there was hardly any detectable [4Fe-4S]¹⁺ species (< 5%) based on Mössbauer and electron paramagnetic resonance (EPR) characterizations of IspG (52, 64). Systematic investigation of IspG catalysis by controlling the reduction potential of the reaction mixture using various redox dyes showed that an optimal IspG activity was obtained at ~450 mV, which is ~150 mV lower than the reduction potential of the flavin cofactor in flavodoxin reductase (52). More importantly, when reduced methyl viologen was employed as the reductant ($E^0 = -446$ mV), IspG activity was increased by 20-fold compared with that of the NADPH-flavodoxin/flavodoxin reductase system (52). Thus, the identity/composition of the *in vivo* IspG reduction system remains to be established.

The challenge of optimal reduction of the IspG iron-sulfur cluster also raises some concerns on the mechanistic relevance of the recently reported IspG paramagnetic species to IspG-catalysis. When dithionite was used as the IspG reductant in steady-state studies, a

paramagnetic species (FeS_A , $g = 2.000, 2.019, \text{ and } 2.087$) was observed (65). FeS_A behaves like high potential iron-sulfur protein (HiPIP) $[\text{4Fe-4S}]^{3+}$ clusters, which have an average EPR g value above 2.0, and remain visible at high temperatures (e.g., 77 K). In a separate pre-steady state study on a thermophilic IspG using dithionite as the reductant, two paramagnetic species (FeS_A and FeS_B in Figure 3B) were detected at 55 °C. One of them is assigned as the enzyme-product complex (FeS_B) (64), and the other (FeS_A) is ascribed to be the same as the one observed in the steady-state studies (65). For this enzyme at 55 °C, a single turnover should be completed in 2 s. However, the signals corresponding to FeS_A are increasing in the first 10–30 s (Figure 3B). The FeS_B species maximizes at 4 min and 7 s and remains discernible even at 16 min (Figure 3B). In contrast, when the best *in vitro* IspG reduction system currently available (reduced methyl viologen) was used at 25 °C, FeS_A is not detected (trace A of Figure 3C) and the FeS_B species (trace C of Figure 3C) is observed within 10 s after the signal from methyl viologen (trace B of Figure 3C) is subtracted from trace A of Figure 3C. When reduced methyl viologen is used as the reductant at 25 °C, 10 s is roughly the time period for a single turnover. Thus, the kinetic properties of FeS_A and FeS_B in Figure 3B and 3C, especially the slow formation and decay of FeS_A (Figure 3B), do not support FeS_A as a kinetically competent intermediate leading to FeS_B formation (Figure 3B) if FeS_B is indeed the IspG-product complex. The fact that only ~1–5% of the IspG iron-sulfur cluster can be reduced when dithionite is used as the direct reductant (64) is clearly a major challenge of current IspG mechanistic studies. Also, the orders of magnitude lower IspG activity when using dithionite as the reductant relative to reduced methyl viologen (52, 64) is another factor that has to be considered in order to properly assign the catalytic relevance of these spectroscopic results.

III.4.3. Mechanistic studies on IspG—One of the major unresolved issues in IspG mechanistic studies is the role of the $[\text{4Fe-4S}]$ cluster in IspG catalysis: 1) involved in substrate activation; 2) as the electron source; or 3) having dual functions in both substrate activation and as the electron source for substrate reduction. Current IspG mechanistic models suggest that the iron-sulfur cluster is involved in substrate activation and also functions as the electron source. The IspG crystal structure indicated that the distance between the proposed MEcPP binding site and its adjacent iron-sulfur cluster on the other IspG subunit is ~20 Å (Figure 3A). If MEcPP directly interacts with the IspG iron-sulfur cluster, MEcPP binding must trigger a conformation change to bring the MEcPP binding site and the iron-cluster close in space for catalysis. In the following section, we will discuss the three IspG mechanistic models, and present currently available biochemical and spectroscopic evidence that support a direct role of the iron-sulfur cluster in IspG-catalysis. The proposed structure for the paramagnetic species FeS_A in *section III. 4.2.* will also be discussed, while the kinetic competence of species FeS_A in IspG catalysis remains as an issue to be studied in the future.

Several IspG mechanistic models have been proposed over the last decade (Figure 4). The epoxide model proposed by Rohdich *et al.* (Figure 4B) involves 2,3-epoxy-4-hydroxy-3-methyl-butenyl 1-diphosphate (**26**) as an intermediate (66). This model is proposed based on the fact that a synthetic $[\text{4Fe-4S}]$ cluster is capable of reductively deoxygenating epoxides to alkenes (67). The first step of the epoxide model is a nucleophilic attack at the C_2 position

by the C₃ hydroxyl group, leading to the ring opening of the cyclic pyrophosphate and the formation of intermediate **26**. The reduced [4Fe-4S]⁺ cluster can then mediate the reductive epoxide ring opening to form a substrate-based radical (**27**). An additional one-electron reduction will generate a carbanion (**28**), which mediates the dehydration to produce HMBPP (**17**). It is not known how the substrate interacts with the iron-sulfur cluster. Coordination of the C₃-OH might facilitate the dehydration step due to the Lewis acidity of the metallo-center. The second and third models share a cation intermediate (**29**, Figure 4C), which was proposed by Seemann and Kollas *et al.* (55, 68). In the cation model, reduction of the cation intermediate (**29**) (69) leads to a radical intermediate (**30**), which undergoes dehydration to **31** through a C-O bond cleavage mechanism as in the case of radical mediated dehydration reactions (70). Coordination of the C₃-OH group of MEcPP (**16**) to the [4Fe-4S] cluster may also facilitate the **30** → **31** transformation as in the case of aconitase (71). Recently, a modified version of the cation model (an organometallic model, Figure 4C) was also proposed based on EPR and electron-nuclear double resonance (ENDOR) characterizations of the paramagnetic FeS_A species discussed in Figure 3B (64, 72, 73). For the organometallic model, the C₂ carbon interacts directly with the [4Fe-4S] cluster unique iron site to form an Fe-C bond (intermediate **32**) and the iron-sulfur cluster is effectively a [4Fe-4S]³⁺ cluster. In the organometallic model, species **32** of Figure 4C was assigned to be the paramagnetic species FeS_A discussed in Figure 3B. Reduction of this organometallic intermediate (**32**) generates HMBPP (**17**) and regenerates the iron-sulfur cluster for the next cycle. Details for the **32** → **17** conversion remains to be clarified and the oxidation state of the [4Fe-4S] cluster unique iron site in intermediate **32** has not yet been studied either.

IspG can utilize the epoxide (**26**) as a substrate as efficiently as MEcPP (**16**) and produce HMBPP (**17**) as the product (Figure 4D) (74). Interestingly, in the absence of reductants, IspG can irreversibly convert **26** to MEcPP (**16**) with a k_{cat} of -2.9 min^{-1} , which is an order of magnitude slower than the steady-state k_{cats} of both the **16** → **17** and **26** → **17** conversions. Since the formation of the epoxide (**26**) has never been detected in the **16** → **17** conversion and the rate of **26** → **17** is roughly 10% of the **16** → **17** conversion (Figure 4D), IspG catalysis may not involve the epoxide (**26**) as an obligate intermediate as proposed in the epoxide model (Figure 4B). These kinetic studies imply that the reductive dehydration of MEcPP (**16**) and reductive deoxygenation of the epoxide (**26**) may proceed through parallel pathways (75). An important question concerning the cation model (Figure 4C) is its energetic feasibility since the C₂ position of MEcPP is unactivated (76). Such C-O bond cleavage was recently examined using the positional isotope exchange method in which [2-¹³C, ¹⁸O]-MEcPP (**16a**) was shown to be converted to **16b** in an IspG-dependent fashion until an equilibrium was reached at the end (Figure 4D). It is known that MEcPP itself is stable for weeks at room temperature and such a positional isotope exchange depends absolutely on the presence of holo-IspG. Since the positional isotope exchange experiment was conducted in the absence of reductants, this result not only provides evidence supporting the reversible C-O bond cleavage at the MEcPP (**16**) C₂ position, but also implies that the formation of a cation intermediate occurs prior to any redox-chemistry (69). How IspG facilitates the MEcPP (**16**) C₂ C-O bond cleavage remains to be addressed.

The above biochemical studies are consistent with the involvement of a cation intermediate (**29**) in IspG catalysis. The downstream chemical reactions after cation formation are still controversial. After the initial report of the FeS_A species by Adedeji *et al.* (65), subsequent studies indicated that the same paramagnetic species (FeS_A) was observed when either the epoxide (**26**) or MEcPP (**16**) was used as the substrate (72, 73). These results can be attributed to the conversion of the epoxide (**26**) to MEcPP (**16**) (Figure 4D) (75). Several additional EPR, ENDOR, and hyperfine sub-level correlation (HYSCORE) spectroscopic studies (64, 72, 73) were reported on the characterization of the paramagnetic species FeS_A , which reveal the following hyperfine tensors: [1.8, 1.6, 1.8] MHz for MEcPP C_5 deuterated methyl group and [14.5, 12.0, 26.5] MHz for the MEcPP C_2 carbon (referring species **32** for the carbon numbering system, Figure 4C). Based on these parameters, Duin, Hoffman and co-workers suggested that such a paramagnetic species (FeS_A) might be either an organometallic species (**32**, Figure 4C) or the IspG-MEcPP complex (**29a**, Figure 4C) (64). Wang *et al.* assigned it as **32** (72, 73). However, since FeS_A formation and decay rates obtained from pre-steady state kinetics (Figure 3B) do not seem to support FeS_A as a kinetically competent species, more systematic kinetic studies are needed in the future. Thus, the exact role of the iron-sulfur cluster and the chemistries after the formation of the cation intermediate (**29**) are not yet known.

III.4.4. Summary—In summary, it is well-accepted that IspG is a unique iron site containing [4Fe-4S] protein based on Mössbauer spectroscopic and X-ray crystallographic characterizations, while it is not yet known how its [4Fe-4S] cluster is involved in substrate activation and catalysis. In the last decade, a combination of a few approaches, including the co-expression of IspG along with *isc* operon and the use of different reduction systems, led to an improvement of IspG activity by a few orders of magnitude. However, other players might be missing as the best IspG activity is still 1 – 2 orders of magnitude less than other MEP pathway enzymes. IspG catalytic mechanisms are still highly controversial. Biochemical studies, especially the positional isotope exchange results, indicate that a cation intermediate might be feasible, while how IspG facilitates the cation formation remains to be addressed. Regarding the intermediates downstream of the proposed cation species (**29**), it is unclear whether the reaction follows the cation radical intermediate (**31**) pathway or the organometallic intermediate (**32**) pathway (Figure 4C). Several reports have emerged recently on the characterization of the paramagnetic species detected in IspG catalysis. Because of the conditions used in these studies, the activity of the enzyme is orders of magnitude less than optimal IspG activity. Thus, the kinetic competency and catalytic relevance of these paramagnetic species to IspG catalysis still need to be established.

III.5. (4-Hydroxy-3-methyl-butenyl 1-diphosphate reductase (IspH))

IspH is an iron-sulfur enzyme (77) catalyzing the reductive dehydration of HMBPP (**17**) to IPP (**1**) and DMAPP (**2**) in a ratio of 5:1 (78). This ratio deviates significantly from the equilibrium ratio (1:3) mediated by IDI (79). Co-expression of IspH with an iron-sulfur maturation system (e.g., *isc* operon) leads to a holo-IspH with activity better than that of *in vitro* reconstituted IspH (80–84). As in the IspG case, when reduced methyl viologen is used as the reduction system, IspH activity can be further improved by two orders of magnitude relative to that of the NADPH-flavodoxin-flavodoxin reductase system (61, 84). Similar to

the case of IspG studies, while significant progress has been made in the last decade, many aspects of IspH catalysis are still highly controversial. IspH mechanistic studies in the last decade will be summarized in three directions: 1) IspH structural flexibility; 2) IspH mechanistic studies; and 3) Stereochemistry in IspH catalysis.

III.5.1. IspH structural flexibility—IspH is a [4Fe-4S] cluster containing protein. Mössbauer spectrum of the [⁵⁷Fe]-labeled IspH is consistent with the presence of a [4Fe-4S]²⁺ cluster having a spin-delocalized Fe^{2.5+}–Fe^{2.5+} pair, and a spin-localized Fe²⁺–Fe³⁺ pair (84, 85). The ferrous site of the spin-localized Fe²⁺–Fe³⁺ pair was proposed to be the substrate binding site. This assignment is supported by the crystal structure of the IspH-HMBPP complex (Figure 5A) (82) and the changes in the isomer shift and quadrupole splitting in the Mössbauer spectrum that are induced by HMBPP binding (online supporting information, Figure 1S and Table 1S) (84–86). Over the last few years, several IspH structures (IspH alone as well as the complex with substrate, products, or substrate analogs, Figure 5) have been reported. One of the important features revealed from these studies is the IspH structural flexibility. In the following section, we will discuss several different IspH conformations.

Most IspH structures determined thus far (IspH alone or in complex with IPP, DMAPP) have a [3Fe-4S]⁺ cluster bound in the active site (Figures 5B and 5C) (82, 87, 88). The recently resolved IspH-HMBPP complex at 1.7 Å resolution has a [4Fe-4S] cluster (Figure 5A) (82), which is coordinated by three conserved Cys residues (Cys12, Cys96, and Cys197 in *E. coli* IspH), with its fourth iron coordinated by the HMBPP C₄-OH group (82). HMBPP (17) itself adopts a hairpin conformation sandwiched between the [4Fe-4S] cluster and its pyrophosphate group in the active site. An H-bonding network is formed through HMBPP, Thr167, Glu126, and an active site bound water. The distance between the HMBPP olefinic carbons (C₂ and C₃, referring Figure 5A for the carbon numbering system) and the [4Fe-4S] cluster unique iron site is 2.8–3.0 Å, shorter than the sum of the van der Waals radii of the iron and carbon atoms (3.6 Å), yet longer than that observed for a typical organometallic iron allylic complex (2.0–2.1 Å) (89). Thus, some interactions between the [4Fe-4S] cluster unique iron site and the HMBPP olefinic moiety are possible. In the IspH-product complex (Figures 5B & 5C) (82), the IPP C₁ adopts an orientation distinct from that of HMBPP (C₁-C₂ bond orientations in Figure 5A vs. 5B). There is also an additional water molecule in the active site (Figure 5A vs. 5B). The differences (Figures 5A, vs. 5B & 5C) in substrate/product orientations in the active site and the number of waters clearly shown that IspH active site is able to adopt a few different conformations.

Prolonged exposure of the IspH-HMBPP complex to X-ray irradiation results in two changes: 1) the distance between C₂ and C₃ of HMBPP to the [4Fe-4S] cluster unique iron site reduces to 2.6–2.8 Å, and 2) the electron-density of the C₄ alkoxide group vanishes (Figure 5D). Such changes are attributed to reductive dehydration of HMBPP, likely triggered by the solvated electrons created by the X-ray photons. The water product from the reductive dehydration may be disordered because no extra water molecule was noted. Interestingly, in the IspH/E126Q-HMBPP complex (Figure 5E), the HMBPP C₄-OH does not co-ordinate to the [4Fe-4S] cluster and instead adopts a completely different conformation; it rotates to the other side of the HMBPP double bond to form an internal H-

bond with its β -phosphate group (90). A similar structure is also implicated in solution by ENDOR spectroscopic analysis of this mutant (see next section for discussion) (91, 92). Whether this conformation (Figure 5E) represents a catalytically relevant intermediate is uncertain since IspH/E126Q mutant is inactive. In addition, the iron-sulfur cluster in this structure (Figure 5E) is in the [3Fe-4S] state instead of the active [4Fe-4S] state. Recently, it was suggested that such a new conformation (Figure 5E) in IspH/E126Q mutant also exists in wild type IspH as a minor species (90).

III.5.2. Mechanistic studies on IspH—Several models have been proposed for IspH catalysis (66, 83, 91, 93–96) (Figure 6). The Birch reduction and organometallic models are the two currently viable mechanisms that are under consideration. In both models, the reaction is initiated by the coordination of HMBPP C₄-OH to the [4Fe-4S]²⁺ unique iron site (33, Figure 6). This step is supported by extensive biochemical (93, 94, 97), Mössbauer (84–86), and crystallographical evidence (82, 95). In the Birch reduction model (66, 82, 84, 93–95), reduction of HMBPP (17) by the reduced [4Fe-4S]⁺ cluster generates a radical anion intermediate (34, Figure 6B), the formation of which triggers C₄-dehydration to an allylic radical-[4Fe-4S]²⁺ intermediate (35). The second one-electron reduction (35 → 36) followed by protonation produces IPP (1) and DMAPP (2) (Route I, Figure 6B). Intermediate 35 may also exist in equilibrium with the allylic anion-[4Fe-4S]³⁺ (37) and its protonation can lead to the product-[4Fe-4S]³⁺ intermediate (38) (Route II, Figure 6B). In the organometallic model, following the initial IspH-HMBPP complex formation (33) (91), the HMBPP olefinic group interacts with the [4Fe-4S] cluster to form a π complex or an η^2 -alkenyl/metallacycle intermediate (39, Figure 6C). Formation of 39 is accompanied by the rotation of HMBPP C₄-OH to the other side of HMBPP double bond to form an internal H-bond with the β -phosphate group as shown in 39. Dehydration of 39 gives an η^1 -allyl intermediate (40), which is likely in equilibrium with an allylic anion-[4Fe-4S]³⁺ species (37). Subsequent reduction and protonation yield IPP (1) and DMAPP (2). The two mechanistic models are similar in many aspects and share several common intermediates (species 33, 37, 38). The main difference between them is the role of the [4Fe-4S] cluster in the catalysis. Besides serving as an anchor to bind the substrate, the [4Fe-4S] cluster in the Birch reduction model carries out reductive dehydration in a stepwise one-electron/one-electron transfer manner. It also functions as a Lewis acid to directly assist the C-O bond cleavage at C₄. The involvement of substrate-based radical intermediates (34 and 35) is specific for the Birch reduction model. In the organometallic model, besides a metallacycle formation (39) triggered ligand replacement and bond-rotation, the other important feature is the iron-sulfur cluster mediated two-electron chemistry. According to the organometallic model, the reductive C-O bond cleavage step (39 → 40) is a two-electron chemistry and the iron-sulfur cluster is oxidized from a [4Fe-4S]⁺ to a [4Fe-4S]³⁺ state. Mössbauer studies indicated that the IspH [4Fe-4S] cluster unique iron is spin localized and is at the +2 state (84–86). Thus, if the redox chemistry is localized at this site, the [4Fe-4S] cluster unique iron oxidation state will go from +2 to +4 state in the reductive C-O bond cleavage step (39 → 40).

Evidence supporting the Birch reduction model is provided by biochemical studies. To assess the energetic contributions of various interactions in the active site during IspH

catalysis and to gain insight into the catalytic mechanism of IspH, a series of substrate analogues were prepared as probes (**41–47**, Table I) (97). The [4-F]-analogue (**41**), which has a fluoro substituent at C₄, can be processed by IspH to produce IPP and DMAPP in a ratio of 7:1 (94). The ~115-fold reduction in $k_{\text{cat}}/K_{\text{m}}$ is proposed to be due to the substitution of the C₄-OH by a fluorine atom, which reduces the proposed interaction between the substrate and the [4Fe-4S] cluster as alkyl fluoride is a poor metal ligand. Similar results were also noted with compound **42**, which has a fluoro group at C₅ instead of C₄, and can be converted by IspH to IPP (**1**) as the sole product. The significant reduction in $k_{\text{cat}}/K_{\text{m}}$ for **42** relative to HMBPP (~1783-fold reduced) is attributed to changes in the hydrogen-bonding network with the active site residues T167 and E126, in addition to the lack of direct coordination of **42** to the [4Fe-4S] cluster (Figure 5A). In fact, a general conclusion emerging from these studies is that the coordination of the C₄-OH of HMBPP to the unique iron site of the [4Fe-4S] cluster is crucial for efficient IspH catalysis. This conclusion supports the Birch reduction model, and is inconsistent with the organometallic model since the involvement of intermediate **39** in catalysis cannot explain the dramatic decrease in catalytic efficiency for mechanistic probe **42** relative to **41** (see Figure 6C and Table I). In addition, the fact that IspH could also utilize the pyrophosphonate analogue (**44**) as a substrate rules out the possibility of a C-O bond scission at the C₁ position as part of the IspH catalysis (94).

More recently, [5-¹³C]-3-(hydroxymethyl)but-3-en-1-yl diphosphate (**43**, Table I) was designed to probe whether **43** shows any preference towards the two possible coordination modes (**48** vs. **51** in Figure 6D) to the [4Fe-4S]²⁺ cluster (97). If the C₄-OH of **43** is the anchor (**48** in Figure 6D), protonation mediated by pyrophosphate at C₄ of the allylic anion intermediate (**49**) would give [¹³C]-IPP (**50**) as the product. In contrast, if the reaction proceeds via an η²-alkenyl intermediate (**51** in Figure 6C), protonation of the allylic anion at the carbon closer to pyrophosphate (now C₅, **52**) should yield [¹³C]-IPP (**53**). The observation that **50** is the sole product after incubation strongly suggests that the C₄-OH group plays the dominant role in orienting the substrate. Indeed, it is confirmed by X-ray crystallography that **43** binds to IspH using its hydroxyl group as the ligand (92). Although biochemical evidences are consistent with the Birch reduction model, none of the key intermediates (**34** – **38**, Figure 6B) have been trapped and characterized.

The organometallic model has been proposed mainly based on EPR characterization of some paramagnetic species. The IspH [4Fe-4S]²⁺ cluster can be reduced by dithionite to a [4Fe-4S]⁺ cluster (77, 91). When IspH E126A or E126Q mutants are reduced by dithionite, a paramagnetic species with *g*-values of 2.124, 1.999, 1.958, is observed (91). The hyperfine parameters obtained from ENDOR characterizations of this species are consistent with the reported structure of IspH/E126Q-HMBPP complex (Figure 5E and **39** in Figure 6B). While the EPR/ENDOR data match the E126Q crystallographic results, the catalytic relevance of this paramagnetic species remains to be verified because the E126 mutants are inactive. Recently, Duin, Hoffman and co-workers reported the observation of a different paramagnetic species with *g* values of 2.173, 2.013, 1.997 using wild type IspH. Such a paramagnetic species was observed upon mixing HMBPP with dithionite pre-reduced IspH (96). The same paramagnetic species was also observed in steady state studies using dithionite as the reductant by Oldfield and co-workers (92). Because the average *g* value is

above 2.0 and the temperature dependence is more like a HiPIP [4Fe-4S]³⁺ cluster, this paramagnetic species was proposed to be the allylic anion-[4Fe-4S]³⁺ intermediate (**37**) (92). To fully establish its chemical nature, one needs to determine its oxidation state. If it is indeed a [4Fe-4S]³⁺ species, the next step is to determine whether it is **37** or the [4Fe-4S]³⁺-product complex (**38**), because the proton source (the pyrophosphate group, Figure 6B) is nearby and the protonation of the substrate-based anionic intermediate (**37**) should be facile. It is also important to note that the IspH turnover number is > 10 s⁻¹ under optimal conditions, and a single turnover should thus be over in 0.1 s (84, 95). The fact that the paramagnetic species with *g* values of 2.173, 2.013, 1.997 was produced on a time scale of seconds to up to tens of minutes (92, 96) casts doubt on its catalytic competency. Thus, more systematic kinetic analysis of these paramagnetic species will be needed.

III.5.3. Stereochemistry in IspH catalysis—Following either the Birch reduction or the organometallic model, protonation of the allylic anion intermediate (**36**) is the last step (Figure 7A). Examination of the structure of the IspH-HMBPP complex (Figure 5A) suggests that the HMBPP pyrophosphate might serve as a potential proton source for C₂ protonation. Such a predicted pro-*S* stereospecificity at the C₂ position was confirmed biochemically recently (98). However, the IPP terminal olefinic methylene stereochemistry remains to be determined (**1a** vs. **1b**, Figure 7B). In the Birch reduction model, the absence of C₃-C₄ bond rotation in **17** suggests IPP (**1a**, Figure 7B) to be the sole product. In contrast, turnover via the organometallic model will give IPP (**1b**) as the anticipated product as a result of the **33** → **39** conversion (Figure 6C). Protonation at C₄ of the allylic intermediate (**36**, Figure 7A) will produce DMAPP (**2a** or **2b**). Again, the DMAPP stereochemistry will depend on whether the reaction involves a C₃-C₄ bond rotation step, and whether pyrophosphate or the water molecule generated from C₄-OH dehydration is the C₄ proton source (Figure 7A). Recently, results of GC-MS analysis of terpenes isolated from a host fed with isotopically labeled deoxyxylulose were cited as evidence supporting the presence of C₃-C₄ bond rotation in IspH catalysis (99). Due to the participation of IPP:DMAPP isomerase (IDI) in the transformation, labeling results from *in vivo* studies are complicated (8, 9, 99–102) and more detailed *in vitro* biochemical studies in the future will provide further evidence to this important mechanistic issue.

III.5.4. Summary—In the last decade, significant progress has been made in IspH catalysis, including the improvement of IspH activity by several orders of magnitude following the optimization of its iron-sulfur cluster maturation and reduction systems. It is well-accepted that HMBPP coordinates to the [4Fe-4S] cluster through its C₄-OH group (**33**, Figure 6), while steps after the HMBPP-IspH complex formation are still highly debated (Birch reduction vs. Organometallic models, Figure 6B and 6C). Trapping and characterizing kinetically competent intermediates and integrating structural, kinetic, spectroscopic, and biochemical information will fill this knowledge gap.

III.6. Type II isopentenyl diphosphate:dimethylallyl diphosphate isomerase (IDI-2)

IPP:DMAPP isomerase (IDI) is responsible for the interconversion between IPP (**1**) and DMAPP (**2**). Although IDI is not essential for the MEP pathway-utilizing organisms, it functions to balance the ratio between IPP and DMAPP to meet the demands under various

cellular conditions. There exist two structurally unrelated IDI enzymes, the type I isomerase (IDI-1) and the type II enzyme (IDI-2). IDI-1 was identified in the 1950s as a Zn²⁺-dependent metalloprotein (103, 104) while IDI-2 was discovered in 2001 (105) and requires reduced flavin mononucleotide (FMN) and Mg²⁺ for activity (105–107). Since isomerization between IPP and DMAPP involves no net change in the redox state of the substrate/product, the exact role of the IDI-2 bound FMN in catalysis has been the focus of extensive research in recent years. Aerobically isolated IDI-II is yellow in color due to the presence of an oxidized FMN coenzyme (105), which can be readily reduced by NADPH or other reductant (e.g., dithionite). Quantitative analysis of NADPH consumption and product formation reveals that only catalytic quantities of NADPH are required to activate the enzyme, after which the reduced IDI-2 remains catalytically competent for multiple turnovers under anaerobic conditions (107, 108).

Most mechanistic studies on IDI-2 focused on differentiating between two mechanisms, a radical model and an acid/base model. The radical model involves the transient flavin semiquinone/substrate radical pair. The acid/based model has a proton addition-elimination mechanism similar to IDI-1. Current evidence supports the mechanistic model in Figure 8A, in which the flavin cofactor functions as acid and base to complete the catalytic cycle. The radical model is less likely based on several lines of evidence. First, despite the detection of a flavin radical in the early study (107), its low concentration and the lack of a corresponding substrate-based radical argue against its catalytic relevance (108, 109). Secondly, stopped-flow studies under single turnover conditions also failed to detect a flavin semiquinone as predicted (109). Finally, no ring-opened or rearrangement product is produced at a detectable level when a few radical clocks (e.g., **54** in Figure 8B) are used (110, 111).

Recent structural, kinetic, and biochemical studies are all consistent with reduced flavin-mediated acid/base chemistry in IDI-2 catalysis (Figure 8A). X-ray crystal structures of the reduced IDI-2 in complex with either IPP or DMAPP reveal a lack of acidic/basic amino acid residues in the vicinity of the substrate (112). Instead, the substrate appears to stack closely on top of the flavin cofactor, with its C₂ atom positioned ~ 3 Å away from N₅ of FMN. Furthermore, the IPP *pro-R* C₂-H, which is stereo-selectively removed during IDI-2 turnover (113), appears to be oriented towards the flavin cofactor N₅ atom. These observations suggest that the reduced FMN coenzyme of IDI-2 may play a direct role in mediating a protonation/deprotonation mechanism. Studies using a series of FMN analogues substituted at the 7- and 8-position of the isoalloxazine moiety with various electron donating and withdrawing groups also strongly support the reduced flavin as an acid/base catalyst (114). Lastly, additional evidence supporting acid/base chemistry was obtained from studies using IDI-2 inhibitors. When epoxide and diene analogues of IPP (**57**, **58**, Figure 8B) were examined, time-dependent IDI-2 inactivation by covalent flavin modification at its C_{4a} position was observed (111, 115–117). Moreover, chiral methyl analysis of the DMAPP products derived from the IDI-2 catalyzed reaction with (*E*)- and (*Z*)-[4-³H]-IPP in D₂O provides strong support for a chemical mechanism involving a flavin-mediated protonation at the vinyl C₄ position of the bound IPP substrate (118). Solvent kinetic isotope effect and proton inventory studies suggest that this proton transfer may be partially rate-limiting

during steady state IDI-2 turnover (118). When taken into consideration with the body of IDI-2 biochemical, kinetic and structural studies, these results are most consistent with a mechanism involving reduced flavin-mediated acid/base chemistry at both C₂ and C₄ of IPP/DMAPP (Figure 8A).

IV. ISOPRENOID PRODUCTION THROUGH METABOLIC ENGINEERING

As one of the most structurally diverse classes of natural products (1, 119), isoprenoids have found applications in areas of medicine (*e.g.*, the antimalarial drug artemisinin (**64**) (2) and the anticancer drug taxol (**68**) (3)), flavor and fragrances (*e.g.*, essential oils (4)), and nutrition (*e.g.*, carotenoids (5)). Plants are one of the major sources of isoprenoids. However, the plant-based supply of isoprenoids suffers from low yields, impurities and the consumption of large amount of natural resources. Due to the structural complexity of many isoprenoids, their chemical syntheses are inherently difficult and costly. For these reasons, the engineering of metabolic pathways for large-scale and cost-effective industrial production presents an attractive alternative source of isoprenoids. Most of the earlier work (up to 2003) on the metabolic engineering of isoprenoids was focused on carotenoids (120). Recent advances in systems biology and synthetic biology (121, 122) including high-throughput screening, low-cost gene synthesis, high speed DNA sequencing, and protein engineering, have enabled the development of commercially-viable, microbial-fermentation processes for isoprenoid production. Thus far, the MVA pathway has been demonstrated to be a superior biosynthetic route for industrial scale isoprenoid production. The current level of MEP pathway-based terpenoid production is substantially lower than that of the engineered MVA pathway. Despite these challenges, there are several potential advantages in pursuing the MEP pathway based isoprenoid production, including a theoretically better stoichiometric yield and less oxygen consumption during fermentation. In this section, we will summarize the lessons learned on metabolic engineering of the MVA and MEP pathways by reviewing two landmark works that led to the high level production of artemisinin precursors (**60** and **63**), and a taxol precursor (**67**, Figure 9).

IV.1. Microbial production of artemisinic acid by engineering the MVA pathway

Artemisinin (**64**, Figure 9), also known as Qinghaosu, is a highly effective antimalarial drug (123) used widely with other anti-malarial drugs in artemisinin-based combination therapies (ACT) (124). The current source of artemisinin is the *Artemisia annua* plant, which is subjected to supply shortages and price volatility. The potential implementation of a global subsidy for ACTs will lead to a significant increase in demand for artemisinin, further exacerbating its already constrained supply (125). It is therefore necessary to find alternative sources of artemisinin to ensure the availability of ACTs to all patients. An attractive route to artemisinin, involving the microbial production of its precursor amorpha-4,11-diene (**60**) or preferably artemisinic acid (**63**, Figure 9), was envisioned early on because a chemical process had been developed to convert amorpha-4,11-diene (**60**) to artemisinin (**64**) via dihydroartemisinic acid (**63**) as an intermediate (126).

The first breakthrough in high-level amorpha-4,11-diene (**60**) production occurred when the MVA pathway from *Saccharomyces cerevisiae* was transplanted into *E. coli* to increase the flux to

farnesyl diphosphate (FPP, **59**, Figure 9) biosynthesis (127). The eight-gene pathway was divided into two operons: the "top" operon (MevT) comprised the first three enzymes converting acetyl-CoA to MVA (**6**, Figure 1A), and the "bottom" operon (MBIS) comprised five enzymes catalyzing the formation of FPP (**59**) from MVA (Figures 1A & 9). Production of amorphadiene (**60**) in a shake-flask reached 24 mg/L in 14 h. Subsequent studies revealed that loss of volatile amorphadiene to evaporation was significant and the development of a two-phase partitioning bioreactor employing dodecane overlay allowed production of 0.5 g/L of amorphadiene (**60**) (128). Additional improvement in amorphadiene production was achieved by detecting and eliminating bottleneck steps that were generated from imbalanced expression of genes resulting from the transfer of a large pathway into a heterologous host. Amorphadiene synthase (AaADS for the **59** → **60** conversion, Figure 9) and mevalonate kinase (MVK for the **6** → **7** conversion, Figure 1A) were identified as two rate-limiting enzymes and optimization of their expression by increasing promoter strength and plasmid copy numbers led to a 7-fold improvement in amorphadiene production (129). Buildup of HMG-CoA (**5**) was observed in the engineered *E. coli* strain, indicating that the activity of HMG-CoA reductase was insufficient to balance the flux (Figure 1A) (130). HMG-CoA accumulation inhibited cell growth and limited the pathway flux. DNA microarray analysis and targeted metabolite profiling revealed that HMG-CoA inhibits fatty acid biosynthesis in the microbial host, leading to generalized membrane stress (131). Subsequent replacement of the *S. cerevisiae* HMG-CoA reductase and HMG-CoA synthase with a more active homolog from *Staphylococcus aureus* eliminated the HMG-CoA accumulation and relieved its toxicity. Coupled with the concomitant fermentation development, high level production of 27 g/L of amorphadiene (**60**) was achieved (132).

For MVA pathway-based isoprenoid production, yeast *S. cerevisiae* is a preferred host over *E. coli* as it employs a native MVA pathway and therefore has no codon bias issues faced by expressing MVA pathway genes in *E. coli*. In addition, many tailoring enzymes in isoprenoid biosynthesis (Figure 9) are cytochrome P450 enzymes and yeast is a better host for their functional expression. When only amorphadiene synthase AaADS (**59** → **60** conversion, Figure 9) was overexpressed under the control of the GAL1 promoter on a high-copy plasmid in *S. cerevisiae* S288C strain, it produced a low quantity of amorphadiene (**60**) (4.4 mg/L) (133). Further improvement of amorphadiene (**60**) yield was achieved by either overexpressing several genes (134) or by overexpressing a transcription factor upc2-1 to globally upregulate the MVA pathway expression (135). Meanwhile, the ergosterol pathway, which competes for FPP, was down-regulated by repression of squalene synthase (ERG9) gene expression. Combination of these efforts elevated the amorphadiene production to 153 mg/L in shake flasks. Subsequent extensive metabolic engineering in conjunction with optimizing fermentation processes culminated in the production of 40 g/L of amorphadiene (**60**) (136). These engineering efforts included: 1) switching the host from S288C to a CEN.PK2 strain, for which physiological information and performance in fermentation is better understood (137); 2) overexpressing the entire MVA pathway by placing all MVA pathway genes under the control of strong GAL promoters, including integrating three copies of HMG-CoA reductase (133); 3) deleting the GAL1 gene to eliminate the utilization of galactose to decrease the fermentation cost (138).

High-level production of amorphadiene (**60**) by fermentation of engineered yeast represents a significant milestone. Microbial production of artemisinic acid (**63**) directly would constitute a superior route toward the development of an economically viable process for the production of semi-synthetic artemisinin (**64**, Figure 9). A cytochrome P450 monooxygenase, CYP71AV1, was isolated from *A. annua* (133, 139) and was found to be able to catalyze all three steps (**60** → **61**, **61** → **62**, and **62** → **63**) needed to oxidize amorphadiene (**60**) to artemisinic acid (**63**). When CYP71AV1 along with its cognate reductase *A. annua* CPR1 (AaCPR1) were expressed in the engineered yeast strain that accumulated 0.5 g/L of amorphadiene (**60**), up to 100 mg/L of artemisinic acid (**63**) was produced (133). Expression of all *A. annua* derived genes (AaADS, CYP71AV1 and AaCPR1) on a single expression plasmid allowed a production of 2.5 g/L of artemisinic acid (**63**) in a galactose-based fermentation process (132). While CYP71AV1 along with its cognate reductase AaCPR1 are capable of performing all three oxidations (**60** → **61**, **61** → **62**, and **62** → **63**), the accumulation of artemisinic aldehyde (**62**) in the fermenters indicated that the conversion of **62** → **63** is not effective. Introducing an aldehyde dehydrogenase (AaALDH1) from *A. annua* in the engineered CEN.PK2 strain eliminated the accumulation of artemisinic aldehyde (**62**) and dramatically increased the production of artemisinic acid **63** to 7.7 g/L (140). Additional expression of an alcohol dehydrogenase (AaADH1) from *A. annua* along with fermentation condition optimization led to titers of 25 g/L of artemisinic acid **63** in 2 L fermenters (141).

IV.2. Production of taxol precursors by engineering the MEP pathway in *E. coli*

MEP pathway engineering for carotenoid (142, 143), sesquiterpene (144, 145), and diterpenoid (146) production has been attempted. The most successful endeavor was the recently reported taxadiene production (**66**, Figure 9) in *E. coli* with a fed-batch fermentation titer of 1 g/L (147). Taxadiene (**66**) is a diterpene precursor for the anticancer drug Taxol (paclitaxel, **68**, Figure 9) (3). The supply of Taxol and its derivatives are constrained by the limitation in its production through plant cell culture-based semi-synthetic processes. Earlier work with *E. coli* engineered for taxadiene (**66**) production by expression of DXS, IDI, GGPP synthase and taxadiene synthase had little success (titer of 1.3 mg/L) (148). The key engineering strategy employed by Ajikumar *et al.* is a focused combinatorial approach designed to identify an optimally balanced pathway while searching a small combinatorial space. To implement this approach, the taxadiene pathway was partitioned into modules separated at the IPP node. The first module comprised eight upstream MEP pathway genes (Figure 1C) but only four (*dxs*, *idi*, *ispD* and *ispF*) were chosen to be modulated. The second module comprised two downstream synthetic genes encoding GGPP synthase and taxadiene synthase for conversion of IPP/DMAPP to taxadiene (Figure 9). The expression of upstream and downstream pathways was modulated by varying the promoters (Trc, T5 and T7) and gene copy numbers, resulting in drastic changes in taxadiene production levels. An unexpected but potentially important result is that a metabolic by-product, indole, showed a negative correlation with taxadiene accumulation. Although it was suggested that there is a possible synergistic effect between indole and isoprenoid pathway intermediates in inhibiting cell growth, the biochemical mechanism of indole interaction with the MEP pathway remains obscure. The best strain identified from the multivariate optimization, however, appeared to have mitigated the

indole's effect and was capable of producing 1 g/L of taxadiene (**66**) in a fed-batch fermentation. Further introduction of a chimeric fusion of taxadiene 5 α -hydroxylase from *Taxus cuspidate* along with its CYP450 reductase into the taxadiene producing strain resulted in the production of 58 mg/L of taxadiene-5 α -ol (**67**, Figure 9) and an equal amount of the by-product 5(12)-oxa-3(11)-cyclotaxane (147). This level of taxadiene-5 α -ol is ~2400-fold higher than previous results. The overall productivity of taxadiene-5 α -ol relative to the taxadiene producing strain, however, was significantly reduced, underscoring the challenge of obtaining efficient hydroxylation reactions in the engineered *E. coli* strain. Although this work represents significant progress in the development of a microbial production platform for taxol, daunting tasks remain because P450-catalyzed conversion of taxadiene to taxadiene-5 α -ol is one of many hydroxylation steps required for the synthesis of taxol (**69**, Figure 9).

IV.3. The MEP versus MVA pathway for metabolic engineering

That nature employs two biosynthetic pathways for isoprenoids not only poses an interesting evolutionary question, but also spurs the debate on which pathway is a better choice for use to engineer microbes for isoprenoid production. Thus far, the MVA pathway has been demonstrated to be a superior biosynthetic route for delivering high-level isoprenoid precursors to terpene synthases for large-scale production, evidenced by the high level production of amorphadiene (**60**) and artemisinic acid (**63**) described above. MEP pathway-based taxadiene production in *E. coli* (147) demonstrated that MEP pathway has the potential to support high flux. The current level of MEP pathway-based terpenoid production is substantially lower than that of the engineered MVA pathway. The limitations of the MEP pathway were initially attributed to unknown regulatory control over the MEP pathway expression in *E. coli*, and later to the accumulation of the metabolic indole caused by the imbalanced pathway expression, leading to the inhibition of the pathway activity (147). However, it is also plausible that the IspG and IspH enzymes may limit the kinetic capacity of the MEP pathway because their *in vitro* activities are 1 – 2 orders of magnitude less than other MEP pathway enzymes.

To avoid the intrinsic regulation mechanism of the MEP pathway in *E. coli*, an obvious and interesting pursuit of the MEP pathway engineering would be its transplantation to an eukaryotic host such as *S. cerevisiae*. Two major challenges exist in building a functional MEP pathway in yeast. Firstly, the functional expression of the two iron-sulfur enzymes (IspG and IspH) is complicated as the yeast cytosol possesses a different Fe-S assembly machinery relative to bacteria (149). A second challenge is faced in the identification of the redox partners required for IspG and IspH activity in yeast. As discussed previously, the exact identities of *in vivo* redox partner proteins (and their corresponding genes) for majority of the IspG and IspH enzymes remain largely unknown. In addition, there are no [2Fe-2S] ferredoxin or flavodoxin homologues to the known ferredoxins (plants) or flavodoxins (bacteria such as *E. coli*) in the cytosol of *S. cerevisiae* (150). An attempt to build a heterologous MEP pathway in *S. cerevisiae* has been described (151), in which the seven genes encoding the *E. coli* MEP pathway were cloned and expressed in *S. cerevisiae* but no redox genes for either IspG or IspH were included. Therefore, it was not surprising that no definitive evidence was presented to demonstrate that the transplanted pathway is functional

in yeast. Despite these challenges, there are several potential advantages in pursuing the MEP pathway based isoprenoid production. First, the MEP pathway provides higher maximal stoichiometric yield from the feedstock than the MVA pathway as it loses less carbon to CO₂ and is also redox balanced. The theoretical mass yield of terpenes from glucose is 30% from DXP (**12**) as compared to 25% from MVA (**6**) (152, 153). Secondly, the MEP pathway requires much less oxygen than the MVA pathway for the production of terpenes, which is economically beneficial to large scale fermentations in which high rates of oxygen delivery can be both challenging and expensive.

V. SUMMARY AND FUTURE DIRECTIONS

V.1. Summary points

1. In the last two decades, two of the most important discoveries in isoprenoid biosynthetic studies are the discovery of the MEP pathway and a modified MVA pathway. Due to the well-defined distribution of the MVA and MEP pathway among different kingdoms, the MEP pathway enzymes have been proposed to be ideal targets for developing new antibiotics and herbicides.
2. Consensus has been reached on the catalytic mechanisms of most MEP pathway enzymes (DXS, DXR, IspD, IspE, and IspF), which are summarized here.
3. For the remaining two enzymes (IspG and IspH), combined efforts from several laboratories have led to an improvement of their *in vitro* activities by several orders of magnitude, while their catalytic mechanisms are still highly debated for at least two reasons: 1) the properties of their iron-sulfur clusters have not been fully elucidated; 2) no kinetically competent intermediates have been trapped and characterized.
4. One of the trends witnessed in the last decade is the shift of focus from demonstrating the ability to make various isoprenoids to industrializing MEP or MVA pathway-based production of isoprenoids *via* microbial fermentations on large scale. Knowledge and tools from several disciplines (e.g., systems biology and protein engineering) are combined to maximize the carbon flux into the desired products.

V.2. Future directions

1. With structural and mechanistic information on almost all MEP pathway enzymes, one of the future focuses is to develop mechanism-based inhibitors and demonstrate their potentials as new antibiotics or herbicides.
2. Several mechanistic issues remain to be resolved for both IspG and IspH: 1) their *in vivo* reduction systems; 2) the functional properties of their iron-sulfur clusters; 3) trapping and characterizing kinetically competent intermediates.

3. MVA-pathway based production of isoprene at a titer of 60 g/L has been achieved, yet it is only at ~11% mass yield and less than half of the maximal yield as calculated for the MVA pathway (153). Achieving maximal yield through enzyme discovery and engineering (147, 154, 155) in conjunction with optimizing microbial fermentation processes will continue to be one of the focuses. Such efforts may allow the development of isoprenoids as renewable chemicals as well as transportation fuels, such as isoprene and farnesene (**72** and **73**, Figure 9) (152, 156–158).
4. Isoprenoid production through MEP pathway based metabolic engineering has several advantages as outlined earlier. Challenges remain in building a functional MEP pathway for isoprenoid production in *E. coli* or yeast, which include the identification of the *in vivo* redox partner proteins (and their corresponding genes) for IspG and IspH, efficient incorporation of iron-sulfur clusters into the engineered strains (*E. coli* or yeast), and the elucidation and manipulation of the intrinsic regulatory mechanisms of the MEP pathway.

Addressing these challenges will not only offer the opportunity to develop new anti-microbial drugs by targeting the MEP pathway enzymes, but also push the engineered microbes to the limit of theoretical yields to produce isoprenoids from renewable feedstocks. The success of these endeavors will help realize the enormous potential of microbes as a sustainable, environmentally friendly solution to the current health, energy, and environmental problems.

Acknowledgments

We are grateful to Prof. JoAnne Stubbe, Dr. Reid McCarty for their critical reading of this manuscript. This work and our research in related areas are supported in part by grants from the National Institutes of Health (GM093903 to P.L. and GM040541 to H.-w.L.), the Welch Foundation (F-1511 to H.w.L.), and NSF CAREER (CHE-0748504 to P.L.).

LIST OF ABBREVIATIONS

DMAPP	Dimethylallyl diphosphate
DXS	1-Deoxy-D-xylulose 5-phosphate synthase
DXP	1-Deoxy-D-xylulose 5-phosphate
DXR (IspC)	DXP reducto-isomerase
EPR	Electron paramagnetic resonance
ENDOR	Electron-nuclear double resonance
GGPP	Geranylgeranyl diphosphate
GPP	Geranyl diphosphate
HiPIP	High potential iron-sulfur protein

HMG-CoA	3-Hydroxy-3-methyl-glutaryl-CoA
HMGR	3-Hydroxy-3-methyl-glutaryl-CoA reductase
HYSCORE	Hyperfine sub-level correlation
IDI	Isopentenyl diphosphate:dimethylallyl diphosphate isomerase
IPP	Isopentenyl diphosphate
IspG	2-C-methyl-D-erythritol-2,4-cyclodiphosphate reductase
IspH	4-Hydroxyl-3-methylbut-2-enyl diphosphate reductase
MEcPP	2-C-methyl-D-erythritol-2,4-cyclodiphosphate
MEP	2-C-methyl-D-erythritol 4-phosphate (methylerythritol phosphate)
MVA	Mevalonate, mevalonic acid
NADPH	Nicotinamide adenine dinucleotide phosphate

REFERENCES

1. Ajikumar PK, Tyo K, Carlsen S, Mucha O, Phon TH, Stephanopoulos G. Terpenoids: opportunities for biosynthesis of natural product drugs using engineered microorganisms. *Mol. Pharm.* 2008; 5:167–190. [PubMed: 18355030]
2. Liu C, Zhao Y, Wang Y. Artemisinin: current state and perspectives for biotechnological production of an antimalarial drug. *Appl. Microbiol. Biotech.* 2006; 72:11–20.
3. Jennewein S, Croteau R. Taxol: biosynthesis, molecular genetics, and biotechnological applications. *Appl. Microbiol. Biotech.* 2001; 57:13–19.
4. Bakkali F, Averbeck S, Averbeck D, Idaomar M. Biological effects of essential oils--a review. *Food Chem. Toxicol.* 2008; 46:446–475. [PubMed: 17996351]
5. Fraser PD, Bramley PM. The biosynthesis and nutritional uses of carotenoids. *Prog. Lipid Res.* 2004; 43:228–265. [PubMed: 15003396]
6. Bloch K. Sterol molecule: structure, biosynthesis, and function. *Steroids.* 1992; 57:378–383. [PubMed: 1519268]
7. Bach TJ. Some new aspects of isoprenoid biosynthesis in plants--a review. *Lipids.* 1995; 30:191–202. [PubMed: 7791527]
8. Eisenreich W, Bacher A, Arigoni D, Rohdich F. Biosynthesis of isoprenoids via the non-mevalonate pathway. *Cell. Mol. Life Sci.* 2004; 61:1401–1426. [PubMed: 15197467]
9. Rohmer M. Diversity in isoprene unit biosynthesis: The methylerythritol phosphate pathway in bacteria and plastids. *Pure Appl. Chem.* 2007; 79:739–751.
10. Rohmer M. The discovery of a mevalonate-independent pathway for isoprenoid biosynthesis in bacteria, algae and higher plants. *Nat. Prod. Rep.* 1999; 16:565–574. [PubMed: 10584331]
11. Hale I, O'Neill PM, Berry NG, Odom A, Sharma R. The MEP pathway and the development of inhibitors as potential anti-infective agents. *MedChemComm.* 2012; 3:418–433.
12. Obiol-Pardo C, Rubio-Martinez J, Imperial S. The methylerythritol phosphate (MEP) pathway for isoprenoid biosynthesis as a target for the development of new drugs against tuberculosis. *Curr. Med. Chem.* 2011; 18:1325–1338. [PubMed: 21366531]
13. Wiemer AJ, Hsiao CH, Wiemer DF. Isoprenoid metabolism as a therapeutic target in gram-negative pathogens. *Curr. Top. Med. Chem.* 2010; 10:1858–1871. [PubMed: 20615187]

14. Gräwert T, Groll M, Rohdich F, Bacher A, Eisenreich W. Biochemistry of the non-mevalonate isoprenoid pathway. *Cell. Mol. Life Sci.* 2011; 68:3797–3814. [PubMed: 21744068]
15. Rohmer, M. *Comprehensive Natural Products II — Chemistry and Biology*. Liu, H-w; Mander, L., editors. Oxford: Elsevier Science Ltd; 2010. p. 517-556.
16. Wiesner J, Jomaa H. Isoprenoid biosynthesis of the apicoplast as drug target. *Curr. Drug Targets.* 2007; 8:3–13. [PubMed: 17266527]
17. Grochowski LL, Xu H, White RH. *Methanocaldococcus jannaschii* uses a modified mevalonate pathway for biosynthesis of isopentenyl diphosphate. *J. Bacteriol.* 2006; 188:3192–3198. [PubMed: 16621811]
18. Chen M, Poulter CD. Characterization of thermophilic archaeal isopentenyl phosphate kinases. *Biochemistry.* 2010; 49:207–217. [PubMed: 19928876]
19. Mabanglo MF, Schubert HL, Chen M, Hill CP, Poulter CD. X-ray structures of isopentenyl phosphate kinase. *ACS Chem. Biol.* 2010; 5:517–527. [PubMed: 20402538]
20. Dellas N, Noel JP. Mutation of archaeal isopentenyl phosphate kinase highlights mechanism and guides phosphorylation of additional isoprenoid monophosphates. *ACS Chem. Biol.* 2010; 5:589–601. [PubMed: 20392112]
21. Rohmer M, Knani M, Simonin P, Sutter B, Sahn H. Isoprenoid biosynthesis in bacteria: a novel pathway for the early steps leading to isopentenyl diphosphate. *Biochem. J.* 1993; 295(Pt 2):517–524. [PubMed: 8240251]
22. Schwarz, H. *Terpene-biosynthese in Gingko biloba: Eine überraschende Geschichte*. Zürich, Switzerland: Eidgenössische Technische Hochschule; 1994.
23. Kuzuyama T, Takagi M, Takahashi S, Seto H. Cloning and characterization of 1-deoxy-D-xylulose 5-phosphate synthase from *Streptomyces* sp strain CL190, which uses both the mevalonate and nonmevalonate pathways for isopentenyl diphosphate biosynthesis. *J. Bacteriol.* 2000; 182:891–897. [PubMed: 10648511]
24. Hahn FM, Eubanks LM, Testa CA, Blagg BSJ, Baker JA, Poulter CD. 1-Deoxy-D-xylulose 5-phosphate synthase, the gene product of open reading frame (ORF) 2816 and ORF 2895 in *Rhodobacter capsulatus*. *J. Bacteriol.* 2001; 183:1–11. [PubMed: 11114895]
25. Xiang S, Usunow G, Lange G, Busch M, Tong L. Crystal structure of 1-deoxy-d-xylulose 5-phosphate synthase, a crucial enzyme for isoprenoids biosynthesis. *J. Biol. Chem.* 2007; 282:2676–2682. [PubMed: 17135236]
26. David S, Estramareix B, Fischer JC, Therisod M. The biosynthesis of thiamine - Syntheses of [1,1,1,5-(²H₄)]-1-deoxy-D-threo-2-pentulose and incorporation of this sugar in biosynthesis of thiazole by *Escherichia coli* cells. *J. Chem. Soc.-Perkin Trans.* 1982:2131–2137.
27. Cane DE, Du S, Robinson JK, Hsiung Y, Spenser ID. Biosynthesis of vitamin B-6: Enzymatic conversion of 1-deoxy-D-xylulose-5-phosphate to pyridoxol phosphate. *J. Am. Chem. Soc.* 1999; 121:7722–7723.
28. Eubanks LM, Poulter CD. *Rhodobacter capsulatus* 1-deoxy-D-xylulose 5-phosphate synthase: Steady-state kinetics and substrate binding. *Biochemistry.* 2003; 42:1140–1149. [PubMed: 12549936]
29. Hoeffler JF, Tritsch D, Grosdemange-Billiard C, Rohmer M. Isoprenoid biosynthesis via the methylerythritol phosphate pathway - Mechanistic investigations of the 1-deoxy-D-xylulose 5-phosphate reductoisomerase. *Eur. J. Biochem.* 2002; 269:4446–4457. [PubMed: 12230556]
30. Proteau PJ. 1-Deoxy-D-xylulose 5-phosphate reductoisomerase: an overview. *Bioorg. Chem.* 2004; 32:483–493. [PubMed: 15530989]
31. Argyrou A, Blanchard JS. Kinetic and chemical mechanism of mycobacterium tuberculosis 1-deoxy-D-xylulose-5-phosphate isomeroreductase. *Biochemistry.* 2004; 43:4375–4384. [PubMed: 15065882]
32. Fox DT, Poulter CD. Mechanistic studies with 2-C-methyl-D-erythritol 4-phosphate synthase from *Escherichia coli*. *Biochemistry.* 2005; 44:8360–8368. [PubMed: 15938625]
33. Wong U, Cox RJ. The chemical mechanism of D-1-deoxyxylulose-5-phosphate reductoisomerase from *Escherichia coli*. *Angew. Chem. Int. Ed.* 2007; 46:4926–4929.

34. Munos JW, Pu X, Mansoorabadi SO, Kim HJ, Liu H-w. A secondary kinetic isotope effect study of the 1-deoxy-D-xylulose-5-phosphate reductoisomerase-catalyzed reaction: evidence for a retroaldol-aldol rearrangement. *J. Am. Chem. Soc.* 2009; 131:2048–2049. [PubMed: 19159292]
35. Mac Sweeney A, Lange R, Fernandes RP, Schulz H, Dale GE, et al. The crystal structure of *E.coli* 1-deoxy-D-xylulose-5-phosphate reductoisomerase in a ternary complex with the antimalarial compound fosmidomycin and NADPH reveals a tight-binding closed enzyme conformation. *J. Mol. Biol.* 2005; 345:115–127. [PubMed: 15567415]
36. Fox DT, Poulter CD. Synthesis and evaluation of 1-deoxy-D-xylulose 5-phosphoric acid analogues as alternate substrates for methylerythritol phosphate synthase. *J. Org. Chem.* 2005; 70:1978–1985. [PubMed: 15760175]
37. Meyer O, Grosdemange-Billiard C, Tritsch D, Rohmer M. Synthesis and activity of two trifluorinated analogues of 1-deoxy-D-xylulose 5-phosphate. *Tetrahedron Lett.* 2007; 48:711–714.
38. Fernandes RPM, Phaosiri C, Proteau PJ. Mutation in the flexible loop of 1-deoxy-D-xylulose 5-phosphate reductoisomerase broadens substrate utilization. *Arch. Biochem. Biophys.* 2005; 444:159–164. [PubMed: 16289362]
39. Munos JW, Pu X, Liu H-w. Synthesis and analysis of a fluorinated product analogue as an inhibitor for 1-deoxy-D-xylulose 5-phosphate reductoisomerase. *Bioorg. Med. Chem. Lett.* 2008; 18:3090–3094. [PubMed: 18078746]
40. Herz S, Wungsintaweekul J, Schuhr CA, Hecht S, Luttgen H, et al. Biosynthesis of terpenoids: YgbB protein converts 4-diphosphocytidyl-2C-methyl-D-erythritol 2-phosphate to 2C-methyl-D-erythritol 2,4-cyclodiphosphate. *Proc. Natl. Acad. Sci. USA.* 2000; 97:2486–2490. [PubMed: 10694574]
41. Rohdich F, Eisenreich W, Wungsintaweekul J, Hecht S, Schuhr CA, Bacher A. Biosynthesis of terpenoids. 2C-methyl-D-erythritol 2,4-cyclodiphosphate synthase (IspF) from *Plasmodium falciparum*. *Eur. J. Biochem.* 2001; 268:3190–3197. [PubMed: 11389720]
42. Testa CA, Lherbet C, Pojer F, Noel JP, Poulter CD. Cloning and expression of IspDF from *Mesorhizobium loti*. Characterization of a bifunctional protein that catalyzes non-consecutive steps in the methylerythritol phosphate pathway. *Biochim. Biophys. Acta Protein Proteomics.* 2006; 1764:85–96.
43. Gabrielsen M, Rohdich F, Eisenreich W, Gräwert T, Hecht S, et al. Biosynthesis of isoprenoids: a bifunctional IspDF enzyme from *Campylobacter jejuni*. *Eur. J. Biochem.* 2004; 271:3028–3035. [PubMed: 15233799]
44. Gabrielsen M, Bond CS, Hallyburton I, Hecht S, Bacher A, et al. Hexameric assembly of the bifunctional methylerythritol 2,4-cyclodiphosphate synthase and protein-protein associations in the deoxy-xylulose-dependent pathway of isoprenoid precursor biosynthesis. *J. Biol. Chem.* 2004; 279:52753–52761. [PubMed: 15466439]
45. Baker J, Franklin DB, Parker J. Sequence and characterization of the gcpE gene of *Escherichia coli*. *FEMS Microbiol. Lett.* 1992; 73:175–180. [PubMed: 1521767]
46. Campos N, Rodríguez-Concepción M, Seemann M, Rohmer M, Boronat A. Identification of gcpE as a novel gene of the 2-C-methyl-D-erythritol 4-phosphate pathway for isoprenoid biosynthesis in *Escherichia coli*. *FEBS Lett.* 2001; 488:170–173. [PubMed: 11163766]
47. Altıncicek B, Kollas AK, Sanderbrand S, Wiesner J, Hintz M, et al. GcpE is involved in the 2-C-methyl-D-erythritol 4-phosphate pathway of isoprenoid biosynthesis in *Escherichia coli*. *J. Bacteriol.* 2001; 183:2411–2416. [PubMed: 11274098]
48. Hecht S, Eisenreich W, Adam P, Amslinger S, Kis K, et al. Studies on the nonmevalonate pathway to terpenes: the role of the GcpE (IspG) protein. *Proc. Natl. Acad. Sci. USA.* 2001; 98:14837–14842. [PubMed: 11752431]
49. Seemann M, Campos N, Rodríguez-Concepción M, Ibañez E, Duvold T, et al. Isoprenoid biosynthesis in *Escherichia coli* via the methylerythritol phosphate pathway: enzymatic conversion of methylerythritol cyclodiphosphate into a phosphorylated derivative of (*E*)-2-methylbut-2-ene-1,4-diol. *Tetrahedron Lett.* 2002; 43:1413–1415.
50. Seemann M, Campos N, Rodríguez-Concepción M, Hoeffler J-F, Grosdemange-Billiard C, et al. Isoprenoid biosynthesis via the methylerythritol phosphate pathway: accumulation of 2-C-methyl-

D-erythritol 2,4-cyclodiphosphate in a *gcpE* deficient mutant of *Escherichia coli*. *Tetrahedron Lett.* 2002; 43:775–778.

51. Zepeck F, Gräwert T, Kaiser J, Schramek N, Eisenreich W, et al. Biosynthesis of isoprenoids. purification and properties of IspG protein from *Escherichia coli*. *J. Org. Chem.* 2005; 70:9168–9174. [PubMed: 16268586]
52. Xiao Y, Zahariou G, Sanakis Y, Liu P. IspG enzyme activity in the deoxyxylulose phosphate pathway: Roles of the iron-sulfur cluster. *Biochemistry.* 2009; 48:10483–10485. [PubMed: 19821611]
53. Johnson DC, Dean DR, Smith AD, Johnson MK. Structure, function, and formation of biological iron-sulfur clusters. *Annu. Rev. Biochem.* 2005; 74:247–281. [PubMed: 15952888]
54. Loiseau L, Gerez C, Bekker M, Ollagnier-de Choudens S, Py B, et al. ErpA, an iron sulfur (Fe S) protein of the A-type essential for respiratory metabolism in *Escherichia coli*. *Proc. Natl. Acad. Sci. USA.* 2007; 104:13626–13631. [PubMed: 17698959]
55. Kollas AK, Duin EC, Eberl M, Altincicek B, Hintz M, et al. Functional characterization of GcpE, an essential enzyme of the non-mevalonate pathway of isoprenoid biosynthesis. *FEBS Lett.* 2002; 532:432–436. [PubMed: 12482607]
56. Seemann M, Wegner P, Schunemann V, Bui BT, Wolff M, et al. Isoprenoid biosynthesis in chloroplasts via the methylerythritol phosphate pathway: the (E)-4-hydroxy-3-methylbut-2-enyl diphosphate synthase (GcpE) from *Arabidopsis thaliana* is a [4Fe-4S] protein. *J. Biol. Inorg. Chem.* 2005; 10:131–137. [PubMed: 15650872]
57. Lee M, Gräwert T, Quitterer F, Rohdich F, Eppinger J, et al. Biosynthesis of isoprenoids: crystal structure of the [4Fe-4S] cluster protein IspG. *J. Mol. Biol.* 2010; 404:600–610. [PubMed: 20932974]
58. Reikittke I, Nonaka T, Wiesner J, Demmer U, Warkentin E, et al. Structure of the E-1-hydroxy-2-methyl-but-2-enyl-4-diphosphate synthase (GcpE) from *Thermus thermophilus*. *FEBS Lett.* 2011; 585:447–451. [PubMed: 21167158]
59. Rees DC, Howard JB. The interface between the biological and inorganic worlds: Iron-sulfur metalloclusters. *Science.* 2003; 300:929–931. [PubMed: 12738849]
60. Beinert H, Holm RH, Munck E. Iron-sulfur clusters: Nature's modular, multipurpose structures. *Science.* 1997; 277:653–659. [PubMed: 9235882]
61. Puan KJ, Wang H, Dairi T, Kuzuyama T, Morita CT. FldA is an essential gene required in the 2-C-methyl-D-erythritol 4-phosphate pathway for isoprenoid biosynthesis. *FEBS Lett.* 2005; 579:3802–3806. [PubMed: 15978585]
62. Seemann M, Tse Sum Bui B, Wolff M, Miginiac-Maslow M, Rohmer M. Isoprenoid biosynthesis in plant chloroplasts via the MEP pathway: direct thylakoid/ferredoxin-dependent photoreduction of GcpE/IspG. *FEBS Lett.* 2006; 580:1547–1552. [PubMed: 16480720]
63. Okada K, Hase T. Cyanobacterial non-mevalonate pathway: (E)-4-hydroxy-3-methylbut-2-enyl diphosphate synthase interacts with ferredoxin in *Thermosynechococcus elongatus* BP-1. *J. Biol. Chem.* 2005; 280:20672–20679. [PubMed: 15792953]
64. Xu W, Lees NS, Adedeji D, Wiesner J, Jomaa H, et al. Paramagnetic intermediates of (E)-4-hydroxy-3-methylbut-2-enyl diphosphate synthase (GcpE/IspG) under steady-state and pre-steady-state conditions. *J. Am. Chem. Soc.* 2010; 132:14509–14520. [PubMed: 20863107]
65. Adedeji D, Hernandez H, Wiesner J, Köhler U, Jomaa H, Duin EC. Possible direct involvement of the active-site [4Fe-4S] cluster of the GcpE enzyme from *Thermus thermophilus* in the conversion of MEcPP. *FEBS Lett.* 2007; 581:279–283. [PubMed: 17214985]
66. Rohdich F, Zepeck F, Adam P, Hecht S, Kaiser J, et al. The deoxyxylulose phosphate pathway of isoprenoid biosynthesis: studies on the mechanisms of the reactions catalyzed by IspG and IspH protein. *Proc. Natl. Acad. Sci. USA.* 2003; 100:1586–1591. [PubMed: 12571359]
67. Itoh T, Nagano T, Sato M, Hirobe M. Deoxygenation of Oxiran Compounds to Olefins by $[\text{Fe}_4\text{S}_4(\text{Sc}_6\text{H}_5)_4]^{2-}$ in the Presence of NaBH_4 . *Tetrahedron Lett.* 1989; 30:6387–6388.
68. Seemann M, Bui BTS, Wolff M, Tritsch D, Campos N, et al. Isoprenoid biosynthesis through the methylerythritol phosphate pathway: The (E)-4-hydroxy-3-methylbut-2-enyl diphosphate synthase (GcpE) is a [4Fe-4S] protein. *Angew. Chem. Int. Ed.* 2002; 41:4337–4339.

69. Xiao Y, Rooker D, You Q, Meyers CLF, Liu P. IspG-Catalyzed Positional Isotopic Exchange in Methylerythritol Cyclodiphosphate of the Deoxyxylulose Phosphate Pathway: Mechanistic Implications. *ChemBiochem*. 2011; 12:527–530. [PubMed: 22238143]
70. Buckel W, Martins BM, Messerschmidt A, Golding BT. Radical-mediated dehydration reactions in anaerobic bacteria. *Biol. Chem*. 2005; 386:951–959. [PubMed: 16218867]
71. Beinert H, Kennedy MC, Stout CD. Aconitase as iron-sulfur protein, enzyme, and iron-regulatory protein. *Chem. Rev*. 1996; 96:2335–2373. [PubMed: 11848830]
72. Wang W, Li J, Wang K, Huang C, Zhang Y, Oldfield E. Organometallic mechanism of action and inhibition of the 4Fe-4S isoprenoid biosynthesis protein GcpE (IspG). *Proc. Natl. Acad. Sci. USA*. 2010; 107:11189–11193. [PubMed: 20534554]
73. Wang W, Wang K, Li J, Nellutla S, Smirnova TI, Oldfield E. An ENDOR and HYSCORE Investigation of a Reaction Intermediate in IspG (GcpE) Catalysis. *J. Am. Chem. Soc*. 2011; 133:8400–8403. [PubMed: 21574560]
74. Nyland RL II, Xiao Y, Liu P, Freil Meyers CL. IspG converts an epoxide substrate analogue to (E)-4-hydroxy-3-methylbut-2-enyl diphosphate: implications for IspG catalysis in isoprenoid biosynthesis. *J. Am. Chem. Soc*. 2009; 131:17734–17735. [PubMed: 19919056]
75. Xiao Y, Nyland RL II, Meyers CL, Liu P. Methylerythritol cyclodiphosphate (MEcPP) in deoxyxylulose phosphate pathway: synthesis from an epoxide and mechanisms. *Chem. Commun*. 2010; 46:7220–7222.
76. Brandt W, Dessoy MA, Fulhorst M, Gao W, Zenk MH, Wessjohann LA. A proposed mechanism for the reductive ring opening of the cyclodiphosphate MEcPP, a crucial transformation in the new DXP/MEP pathway to isoprenoids based on modeling studies and feeding experiments. *ChemBiochem*. 2004; 5:311–323. [PubMed: 14997523]
77. Wolff M, Seemann M, Bui BTS, Frapart Y, Tritsch D, et al. Isoprenoid biosynthesis via the methylerythritol phosphate pathway: the (E)-4-hydroxy-3-methylbut-2-enyl diphosphate reductase (LytB/IspH) from *Escherichia coli* is a [4Fe-4S] protein. *FEBS Lett*. 2003; 541:115–120. [PubMed: 12706830]
78. Rohdich F, Hecht S, Gärtner K, Adam P, Krieger C, et al. Studies on the nonmevalonate terpene biosynthetic pathway: Metabolic role of IspH (LytB) protein. *Proc. Natl. Acad. Sci. USA*. 2002; 99:1158–1163. [PubMed: 11818558]
79. Street IP, Christensen DJ, Poulter CD. Hydrogen-exchange during the enzyme-catalyzed isomerization of isopentenyl diphosphate and dimethylallyl diphosphate. *J. Am. Chem. Soc*. 1990; 112:8577–8578.
80. Adam P, Hecht S, Eisenreich WG, Kaiser J, Gräwert T, et al. Biosynthesis of terpenes: Studies on 1-hydroxy-2-methyl-2-(E)-butenyl 4-diphosphate reductase. *Proc. Natl. Acad. Sci. USA*. 2002; 99:12108–12113. [PubMed: 12198182]
81. Gräwert T, Kaiser J, Zepeck F, Laupitz R, Hecht S, et al. IspH protein of *Escherichia coli*: Studies on iron-sulfur cluster implementation and catalysis. *J. Am. Chem. Soc*. 2004; 126:12847–12855. [PubMed: 15469281]
82. Gräwert T, Span I, Eisenreich W, Rohdich F, Eppinger J, et al. Probing the reaction mechanism of IspH protein by x-ray structure analysis. *Proc. Natl. Acad. Sci. USA*. 2010; 107:1077–1081. [PubMed: 20080550]
83. Altıncicek B, Duin EC, Reichenberg A, Hedderich R, Kollas AK, et al. LytB protein catalyzes the terminal step of the 2-C-methyl-D-erythritol-4-phosphate pathway of isoprenoid biosynthesis. *FEBS Lett*. 2002; 532:437–440. [PubMed: 12482608]
84. Xiao Y, Chu L, Sanakis Y, Liu P. Revisiting the IspH catalytic system in the deoxyxylulose phosphate pathway: achieving high activity. *J. Am. Chem. Soc*. 2009; 131:9931–9933. [PubMed: 19583210]
85. Seemann M, Janthawornpong K, Schweizer J, Böttger LH, Janoschka A, et al. Isoprenoid biosynthesis via the MEP pathway: *In vivo* Mössbauer spectroscopy identifies a [4Fe-4S]²⁺ center with unusual coordination sphere in the LytB protein. *J. Am. Chem. Soc*. 2009; 131:13184–13185. [PubMed: 19708647]

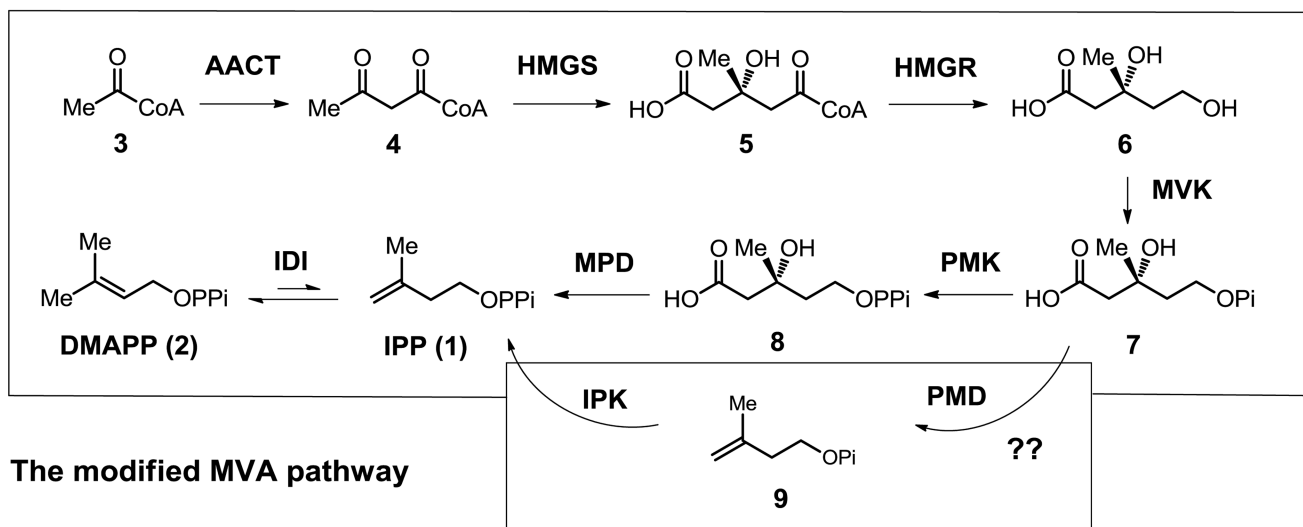
86. Ahrens-Botzong A, Janthawornpong K, Wolny JA, Tambou EN, Rohmer M, et al. Biosynthesis of isoprene units: Mössbauer spectroscopy of substrate and inhibitor binding to the [4Fe-4S] cluster of the LytB/IspH enzyme. *Angew. Chem. Int. Ed.* 2011; 50:11976–11979.
87. Rekkittke I, Wiesner J, Röhrich R, Demmer U, Warkentin E, et al. Structure of (E)-4-hydroxy-3-methyl-but-2-enyl diphosphate reductase, the terminal enzyme of the non-mevalonate pathway. *J. Am. Chem. Soc.* 2008; 130:17206–17207. [PubMed: 19035630]
88. Gräwert T, Rohdich F, Span I, Bacher A, Eisenreich W, et al. Structure of active IspH enzyme from *Escherichia coli* provides mechanistic insights into substrate reduction. *Angew. Chem. Int. Ed.* 2009; 48:5756–5759.
89. Bolm C, Legros J, Le Paih J, Zani L. Iron-catalyzed reactions in organic synthesis. *Chem. Rev.* 2004; 104:6217–6254. [PubMed: 15584700]
90. Span I, Grawert T, Bacher A, Eisenreich W, Groll M. Crystal structures of mutant IspH proteins reveal a rotation of the substrate's hydroxymethyl group during catalysis. *J. Mol. Biol.* 2012; 416:1–9. [PubMed: 22137895]
91. Wang WX, Wang K, Liu YL, No JH, Li JK, et al. Bioorganometallic mechanism of action, and inhibition, of IspH. *Proc. Natl. Acad. Sci. USA.* 2010; 107:4522–4527. [PubMed: 20173096]
92. Wang W, Wang K, Span I, Jauch J, Bacher A, et al. Are free radicals involved in IspH catalysis? An EPR and crystallographic investigation. *J. Am. Chem. Soc.* 2012; 134:11225–11234. [PubMed: 22687151]
93. Xiao Y, Liu P. IspH protein of the deoxyxylulose phosphate pathway: mechanistic studies with C₁-deuterium-labeled substrate and fluorinated analogue. *Angew. Chem. Int. Ed.* 2008; 47:9722–9725.
94. Xiao Y, Zhao ZK, Liu P. Mechanistic studies of IspH in the deoxyxylulose phosphate pathway: Heterolytic C-O bond cleavage at C-4 position. *J. Am. Chem. Soc.* 2008; 130:2164–2165. [PubMed: 18217765]
95. Gräwert T, Span I, Bacher A, Groll M. Reductive dehydroxylation of allyl alcohols by IspH protein. *Angew. Chem. Int. Ed.* 2010; 49:8802–8809.
96. Xu W, Lees NS, Hall D, Welideniya D, Hoffman BM, Duin EC. A closer look at the spectroscopic properties of possible reaction intermediates in wild-type and mutant (E)-4-hydroxy-3-methylbut-2-enyl diphosphate reductase. *Biochemistry.* 2012; 51:4845–4849.
97. Chang, W-c; Xiao, Y.; Liu, H-w; Liu, P. Mechanistic studies of an IspH-catalyzed reaction: Implications for substrate binding and protonation in the biosynthesis of isoprenoids. *Angew. Chem. Int. Ed.* 2011; 50:12304–12307.
98. Laupitz R, Gräwert T, Rieder C, Zepeck F, Bacher A, et al. Stereochemical studies on the making and unmaking of isopentenyl diphosphate in different biological systems. *Chemistry & Biodiversity.* 2004; 1:1367–1376. [PubMed: 17191914]
99. Citron CA, Brock NL, Rabe P, Dickschat JS. The stereochemical course and mechanism of the IspH reaction. *Angew. Chem. Int. Ed.* 2012; 51:4053–4057.
100. Arigoni D, Eisenreich W, Latzel C, Sagner S, Radykewicz T, et al. Dimethylallyl pyrophosphate is not the committed precursor of isopentenyl pyrophosphate during terpenoid biosynthesis from 1-deoxyxylulose in higher plants. *Proc. Natl. Acad. Sci. USA.* 1999; 96:1309–1314. [PubMed: 9990020]
101. Rieder C, Jaun B, Arigoni D. On the early steps of cineol biosynthesis in *Eucalyptus globulus*. *Helv. Chim. Acta.* 2000; 83:2504–2513.
102. Tritsch D, Hemmerlin A, Bach TJ, Rohmer M. Plant isoprenoid biosynthesis via the MEP pathway: *In vivo* IPP/DMAPP ratio produced by (E)-4-hydroxy-3-methylbut-2-enyl diphosphate reductase in tobacco BY-2 cell cultures. *FEBS Lett.* 2010; 584:129–134. [PubMed: 19903472]
103. Agranoff BW, Eggerer H, Henning U, Lynen F. Isopentenyl pyrophosphate isomerase. *J. Am. Chem. Soc.* 1959; 81:1254–1255.
104. Agranoff BW, Eggerer H, Henning U, Lynen F. Biosynthesis of terpenes. VII. Isopentenyl pyrophosphate isomerase. *J. Biol. Chem.* 1960; 235:326–332. [PubMed: 13792054]
105. Kaneda K, Kuzuyama T, Takagi M, Hayakawa Y, Seto H. An unusual isopentenyl diphosphate isomerase found in the mevalonate pathway gene cluster from *Streptomyces* sp strain CL190. *Proc. Natl. Acad. Sci. USA.* 2001; 98:932–937. [PubMed: 11158573]

106. Hemmi H, Ikeda Y, Yamashita S, Nakayama T, Nishino T. Catalytic mechanism of type 2 isopentenyl diphosphate : dimethylallyl diphosphate isomerase: verification of a redox role of the flavin cofactor in a reaction with no net redox change. *Biochem. Biophys. Res. Commun.* 2004; 322:905–910. [PubMed: 15336549]
107. Kittleman W, Thibodeaux CJ, Liu YN, Zhang H, Liu H-w. Characterization and mechanistic studies of type II isopentenyl diphosphate : dimethylallyl diphosphate isomerase from *Staphylococcus aureus*. *Biochemistry.* 2007; 46:8401–8413. [PubMed: 17585782]
108. Rothman SC, Helm TR, Poulter CD. Kinetic and spectroscopic characterization of type II isopentenyl diphosphate isomerase from *Thermus thermophilus*: Evidence for formation of substrate-induced flavin species. *Biochemistry.* 2007; 46:5437–5445. [PubMed: 17428035]
109. Thibodeaux CJ, Mansoorabadi SO, Kittleman W, Chang W-c, Liu H-w. Evidence for the involvement of acid/base chemistry in the reaction catalyzed by the type II isopentenyl diphosphate/dimethylallyl diphosphate isomerase from *Staphylococcus aureus*. *Biochemistry.* 2008; 47:2547–2558. [PubMed: 18229948]
110. Johnston JB, Walker JR, Rothman SC, Poulter CD. Type-2 isopentenyl diphosphate isomerase. Mechanistic studies with cyclopropyl and epoxy analogues. *J. Am. Chem. Soc.* 2007; 129:7740–7741. [PubMed: 17547410]
111. Rothman SC, Johnston JB, Lee S, Walker JR, Poulter CD. Type II isopentenyl diphosphate isomerase: Irreversible inactivation by covalent modification of flavin. *J. Am. Chem. Soc.* 2008; 130:4906–4913. [PubMed: 18345677]
112. Unno H, Yamashita S, Ikeda Y, Sekiguchi S, Yoshida N, et al. New role of flavin as a general acid-base catalyst with no redox function in Type 2 isopentenyl-diphosphate isomerase. *J. Biol. Chem.* 2009; 284:9160–9167. [PubMed: 19158086]
113. Kao CL, Kittleman W, Zhang H, Seto H, Liu H-w. Stereochemical analysis of isopentenyl diphosphate isomerase type II from *Staphylococcus aureus* using chemically synthesized (*S*)- and (*R*)-[2-²H]isopentenyl diphosphates. *Org. Lett.* 2005; 7:5677–5680. [PubMed: 16321020]
114. Thibodeaux CJ, Chang W-c, Liu H-w. Linear Free Energy Relationships Demonstrate a Catalytic Role for the Flavin Mononucleotide Coenzyme of the Type II Isopentenyl Diphosphate:Dimethylallyl Diphosphate Isomerase. *J. Am. Chem. Soc.* 2010; 132:9994–9996. [PubMed: 20593767]
115. Walker JR, Rothman SC, Poulter CD. Synthesis and evaluation of substrate analogues as mechanism-based inhibitors of type II isopentenyl diphosphate isomerase. *J. Org. Chem.* 2008; 73:726–729. [PubMed: 18088143]
116. Nagai T, Unno H, Janczak MW, Yoshimura T, Poulter CD, Hemmi H. Covalent modification of reduced flavin mononucleotide in type-2 isopentenyl diphosphate isomerase by active-site-directed inhibitors. *Proc. Natl. Acad. Sci. USA.* 2011; 108:20461–20466. [PubMed: 22158896]
117. Hoshino T, Tamegai H, Kakinuma K, Eguchi T. Inhibition of type 2 isopentenyl diphosphate isomerase from *Methanocaldococcus jannaschii* by a mechanism-based inhibitor of type I isopentenyl diphosphate isomerase. *Bioorg. Med. Chem.* 2006; 14:6555–6559. [PubMed: 16793276]
118. Calveras J, Thibodeaux CJ, Mansoorabadi SO, Liu H-w. Stereochemical Studies of the Type II Isopentenyl Diphosphate-Dimethylallyl Diphosphate Isomerase Implicate the FMN Coenzyme in Substrate Protonation. *ChemBiochem.* 2012; 13:42–46. [PubMed: 22135039]
119. Breitmaier, E. Terpenes: Flavors, Fragrances, Pharmaca, Pheromones. Weinheim, Germany: WILEY-VCH; 2006.
120. Barkovich R, Liao JC. Metabolic engineering of isoprenoids. *Metab. Eng.* 2001; 3:27–39. [PubMed: 11162230]
121. Fu, P.; Panke, S. Systems biology and synthetic biology. Weinheim, Germany: WILEY-VCH; 2009.
122. Tyo KE, Alper HS, Stephanopoulos GN. Expanding the metabolic engineering toolbox: more options to engineer cells. *Trends Biotech.* 2007; 25:132–137.
123. White NJ. Qinghaosu (artemisinin): the price of success. *Science.* 2008; 320:330–334. [PubMed: 18420924]
124. Olumese P. Guidelines for the treatment of malaria. World Health Organization. 2006

125. Van Noorden R. Demand for malaria drug soars. *Nature*. 2010; 466:672–673. [PubMed: 20686539]
126. Hale V, Keasling JD, Renninger N, Diagana TT. Microbially derived artemisinin: a biotechnology solution to the global problem of access to affordable antimalarial drugs. *Am. J. Trop. Med. Hyg.* 2007; 77:198–202. [PubMed: 18165493]
127. Martin VJ, Pitera DJ, Withers ST, Newman JD, Keasling JD. Engineering a mevalonate pathway in *Escherichia coli* for production of terpenoids. *Nat. Biotechnol.* 2003; 21:796–802. [PubMed: 12778056]
128. Newman JD, Marshall J, Chang M, Nowroozi F, Paradise E, et al. High-level production of amorpha-4,11-diene in a two-phase partitioning bioreactor of metabolically engineered *Escherichia coli*. *Biotechnol. Bioeng.* 2006; 95:684–691. [PubMed: 16878333]
129. Anthony JR, Anthony LC, Nowroozi F, Kwon G, Newman JD, Keasling JD. Optimization of the mevalonate-based isoprenoid biosynthetic pathway in *Escherichia coli* for production of the antimalarial drug precursor amorpha-4,11-diene. *Metab. Eng.* 2009; 11:13–19. [PubMed: 18775787]
130. Pitera DJ, Paddon CJ, Newman JD, Keasling JD. Balancing a heterologous mevalonate pathway for improved isoprenoid production in *Escherichia coli*. *Metab. Eng.* 2007; 9:193–207. [PubMed: 17239639]
131. Kizer L, Pitera DJ, Pflieger BF, Keasling JD. Application of functional genomics to pathway optimization for increased isoprenoid production. *Appl. Environ. Microbiol.* 2008; 74:3229–3241. [PubMed: 18344344]
132. Lenihan JR, Tsuruta H, Diola D, Renninger NS, Regentin R. Developing an industrial artemisinic acid fermentation process to support the cost-effective production of antimalarial artemisinin-based combination therapies. *Biotechnol. Prog.* 2008; 24:1026–1032. [PubMed: 19194910]
133. Ro DK, Paradise EM, Ouellet M, Fisher KJ, Newman KL, et al. Production of the antimalarial drug precursor artemisinic acid in engineered yeast. *Nature*. 2006; 440:940–943. [PubMed: 16612385]
134. Donald KA, Hampton RY, Fritz IB. Effects of overproduction of the catalytic domain of 3-hydroxy-3-methylglutaryl coenzyme A reductase on squalene synthesis in *Saccharomyces cerevisiae*. *Appl. Environ. Microbiol.* 1997; 63:3341–3344. [PubMed: 9292983]
135. Davies BS, Wang HS, Rine J. Dual activators of the sterol biosynthetic pathway of *Saccharomyces cerevisiae*: similar activation/regulatory domains but different response mechanisms. *Mol Cell. Biol.* 2005; 25:7375–7385. [PubMed: 16055745]
136. Westfall PJ, Pitera DJ, Lenihan JR, Eng D, Woolard F, et al. Production of Amorphadiene in yeast, and its conversion to dihydroartemisinic acid, precursor to the antimalarial agent artemisinin. *Proc. Natl. Acad. Sci. USA.* 2012; 109:E111–E118. [PubMed: 22247290]
137. van Dijken JP, Bauer J, Brambilla L, Duboc P, Francois JM, et al. An interlaboratory comparison of physiological and genetic properties of four *Saccharomyces cerevisiae* strains. *Enzyme Microb. Tech.* 2000; 26:706–714.
138. Hovland P, Flick J, Johnston M, Sclafani RA. Galactose as a gratuitous inducer of GAL gene expression in yeasts growing on glucose. *Gene.* 1989; 83:57–64. [PubMed: 2512199]
139. Teoh KH, Polichuk DR, Reed DW, Nowak G, Covello PS. *Artemisia annua* L. (Asteraceae) trichome-specific cDNAs reveal CYP71AV1, a cytochrome P450 with a key role in the biosynthesis of the antimalarial sesquiterpene lactone artemisinin. *FEBS Lett.* 2006; 580:1411–1416. [PubMed: 16458889]
140. Teoh KH, Polichuk DR, Reed DW, Covello PS. Molecular cloning of an aldehyde dehydrogenase implicated in artemisinin biosynthesis in *Artemisia annua*. *Botany.* 2009; 87:635–642.
141. Tsuruta H, Paddon CJ, Eng D, Lenihan JR, Horning T, et al. High-level production of amorpha-4,11-diene, a precursor of the antimalarial agent artemisinin, in *Escherichia coli*. *PLoS One.* 2009; 4:e4489. [PubMed: 19221601]
142. Farmer WR, Liao JC. Precursor balancing for metabolic engineering of lycopene production in *Escherichia coli*. *Biotechnol. Prog.* 2001; 17:57–61. [PubMed: 11170480]
143. Kim SW, Keasling JD. Metabolic engineering of the nonmevalonate isopentenyl diphosphate synthesis pathway in *Escherichia coli* enhances lycopene production. *Biotechnol. Bioeng.* 2001; 72:408–415. [PubMed: 11180061]

144. Martin VJ, Yoshikuni Y, Keasling JD. The *in vivo* synthesis of plant sesquiterpenes by *Escherichia coli*. *Biotechnol. Bioeng.* 2001; 75:497–503. [PubMed: 11745124]
145. Cane DE, Wu Z, Oliver JS, Hohn TM. Overproduction of soluble trichodiene synthase from *Fusarium sporotrichioides* in *Escherichia coli*. *Arch. Biochem. Biophys.* 1993; 300:416–422. [PubMed: 8424673]
146. Morrone D, Lowry L, Determan MK, Hershey DM, Xu M, Peters RJ. Increasing diterpene yield with a modular metabolic engineering system in *E. coli*: comparison of MEV and MEP isoprenoid precursor pathway engineering. *Appl. Microbiol. Biotech.* 2010; 85:1893–1906.
147. Ajikumar PK, Xiao WH, Tyo KE, Wang Y, Simeon F, et al. Isoprenoid pathway optimization for Taxol precursor overproduction in *Escherichia coli*. *Science.* 2010; 330:70–74. [PubMed: 20929806]
148. Huang Q, Roessner CA, Croteau R, Scott AI. Engineering *Escherichia coli* for the synthesis of taxadiene, a key intermediate in the biosynthesis of taxol. *Bioorg. Med. Chem.* 2001; 9:2237–2242. [PubMed: 11553461]
149. Lill R, Muhlenhoff U. Maturation of iron-sulfur proteins in eukaryotes: mechanisms, connected processes, and diseases. *Annu. Rev. Biochem.* 2008; 77:669–700. [PubMed: 18366324]
150. Liger D, Graille M, Zhou CZ, Leulliot N, Quevillon-Cheruel S, et al. Crystal structure and functional characterization of yeast YLR011wp, an enzyme with NAD(P)H-FMN and ferric iron reductase activities. *J. Biol. Chem.* 2004; 279:34890–34897. [PubMed: 15184374]
151. Maury J, Asadollahi MA, Moller K, Schalk M, Clark A, et al. Reconstruction of a bacterial isoprenoid biosynthetic pathway in *Saccharomyces cerevisiae*. *FEBS Lett.* 2008; 582:4032–4038. [PubMed: 18996117]
152. Rude MA, Schirmer A. New microbial fuels: a biotech perspective. *Curr. Opin. Microbiol.* 2009; 12:274–281. [PubMed: 19447673]
153. Whited GM, Feher FJ, Benko DA, Cervin MA, Chotani GK, et al. TECHNOLOGY UPDATE: Development of a gas-phase bioprocess for isoprene-monomer production using metabolic pathway engineering. *Ind. Biotechnol.* 2010; 6:152–163.
154. Cane DE. Enzymatic formation of sesquiterpenes. *Chem. Rev.* 1990; 90:1089–1103.
155. Chang MC, Eachus RA, Trieu W, Ro DK, Keasling JD. Engineering *Escherichia coli* for production of functionalized terpenoids using plant P450s. *Nat. Chem. Biol.* 2007; 3:274–277. [PubMed: 17438551]
156. Zhang F, Rodriguez S, Keasling JD. Metabolic engineering of microbial pathways for advanced biofuels production. *Curr. Opin. Biotechnol.* 2011; 22:1–9. [PubMed: 21190838]
157. Renninger, NS.; Mcphee, DJ., inventors. Patent No. US. 2008045555. 2008.
158. Tsuruta, H.; Lenihan, JR.; Regentin, R., inventors. Patent No WO. 2009042070A2. 2009.

A. The MVA pathway



B. The modified MVA pathway

C. The MEP pathway

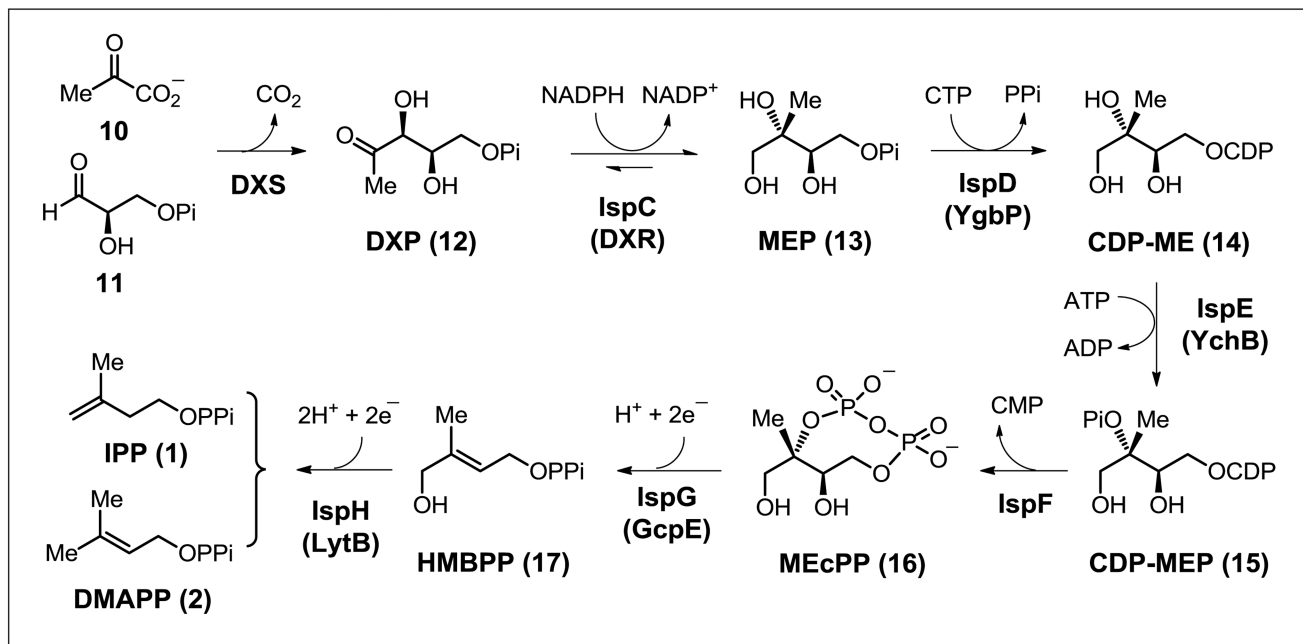
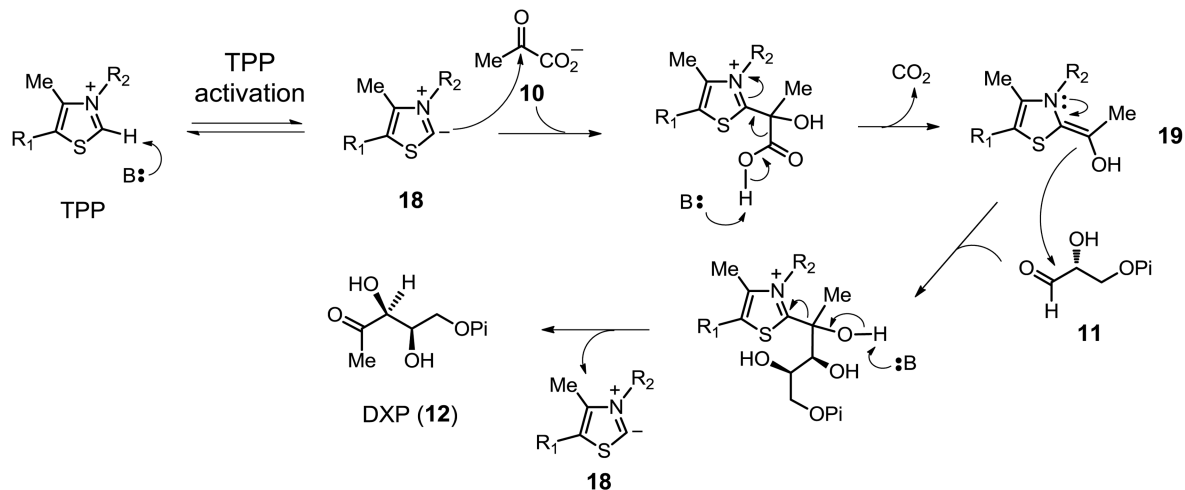
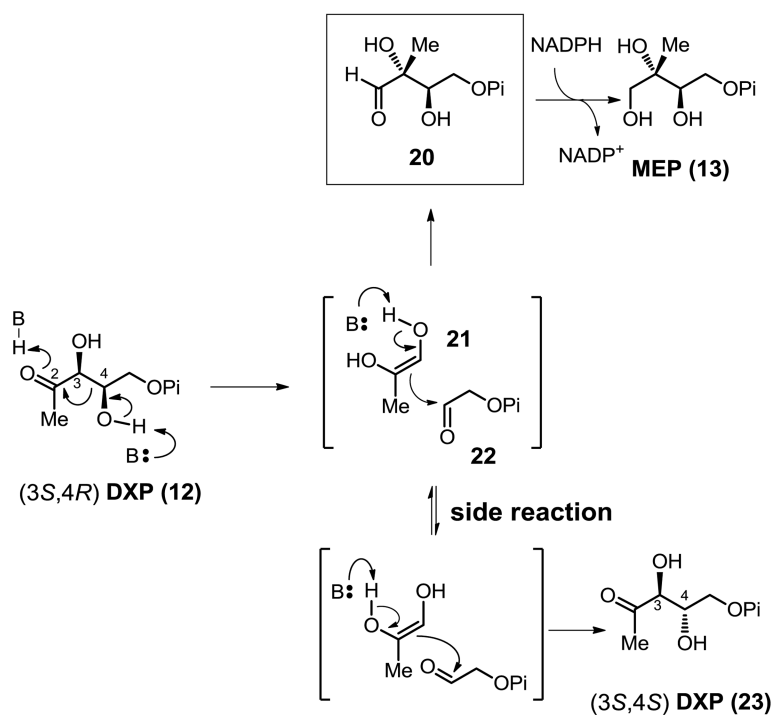


Figure 1. Pathways for the biosyntheses of isoprenoid precursors (IPP and DMAPP) and their well-defined distributions among different kingdoms. **A.** The mevolanate pathway (MVA pathway) in animals, plants (cytosol), fungi, and archaea; **B.** The modified MVA pathway in *Methanocaldococcus jannaschii*; **C.** The methylerythritol phosphate pathway (MEP pathway) in eubacteria, green algae, and the plastids of higher plants.

A. DXS Mechanism



B. DXR Mechanistic Model: Retroaldol/aldol Rearrangement



C. IspF Catalyzed Reactions

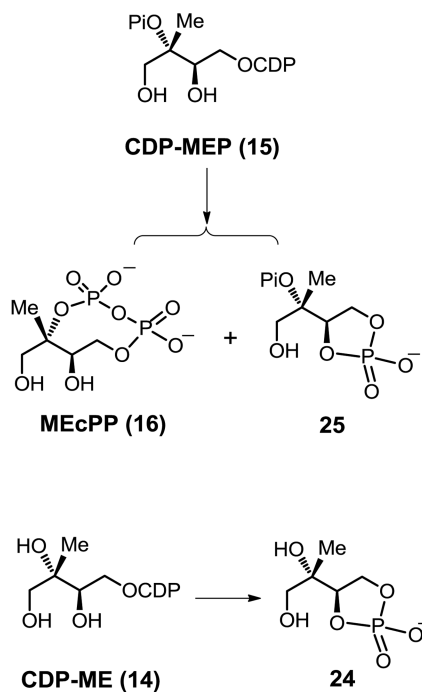


Figure 2.

A. Mechanism of TPP mediated condensation between pyruvate (**10**) and glyceraldehyde 3-phosphate (**11**) in DXS catalysis. **B.** The DXR retro-aldol/aldol rearrangement mechanistic model. In the retro-aldol/aldol model, a side reaction may occur through the C-C bond rotation in fragment **22** followed by the recombination between **21** and **22** to produce (3*S*, 4*S*)-DXP (**23**), a stereo-isomer of the DXR native substrate (3*S*, 4*R*)-DXP (**12**). **C.** Unique IspF-chemistries. Besides the native IspF catalysis (**15** → **16** conversion), two more IspF chemistries (**14** → **24** and **15** → **25** conversions) are discovered in some organisms.

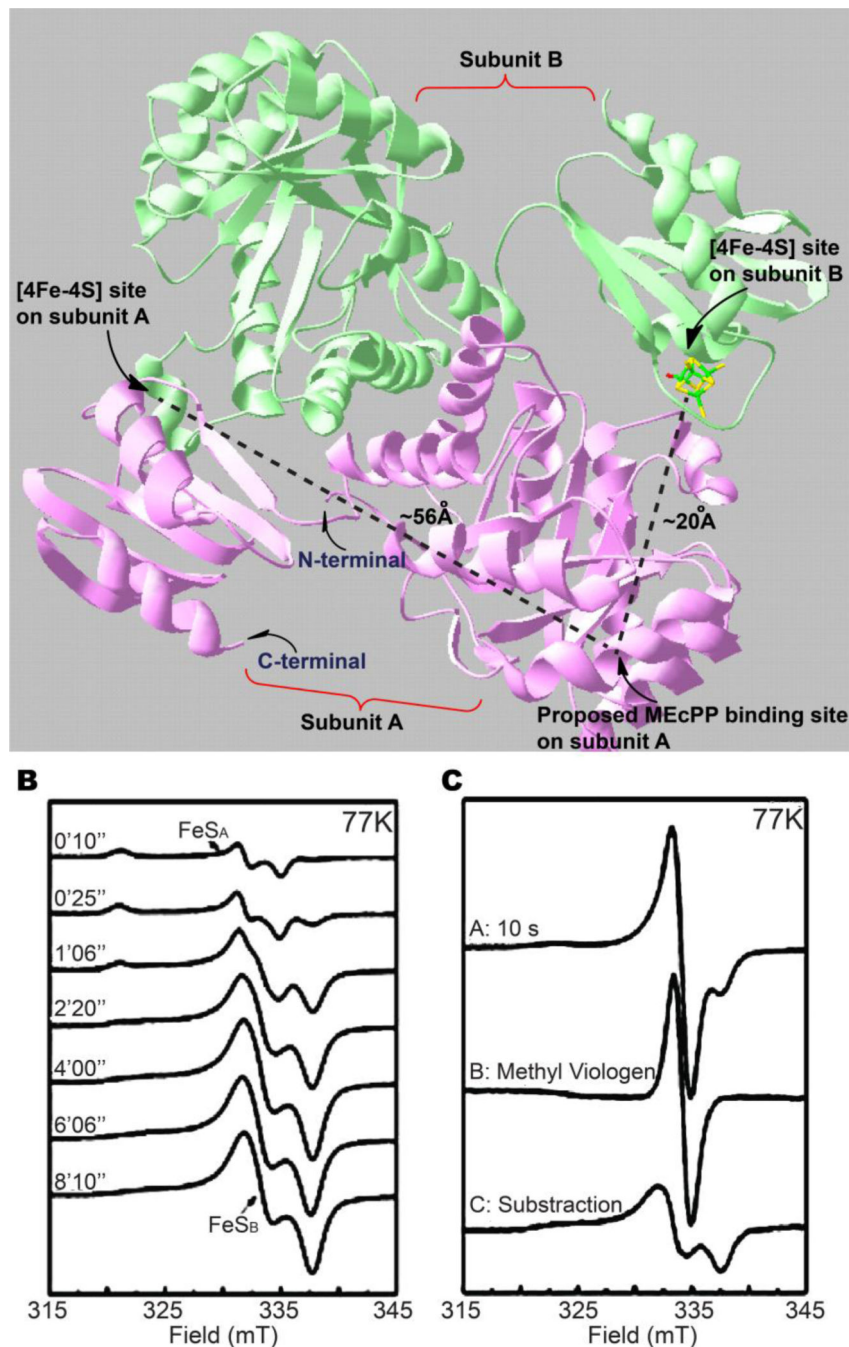


Figure 3. X-ray crystallographic and EPR spectroscopic characterizations of IspG. **A.** Structure of *Aquifex aeolicus* IspG. IspG is a homodimer assembled in a head-to tail fashion. Each subunit has two domains, the proposed MECPP binding *N*-terminal domain and the *C*-terminal [4Fe-4S] cluster domain. The proposed IspG active site is located at the interface between the *N*-terminal of one subunit and the *C*-terminal of the other subunit as the distance between the MECPP binding site and the [4Fe-4S] cluster within the same subunit is too far (~56 Å). **B.** Pre-steady state characterizations of a thermophilic IspG using dithionite

as the reductant at 55 °C. **C.** Pre-steady state characterizations of a thermophilic IspG using reduced methylviologen as the reductant. A single turnover at 25 °C takes ~ 10 s, which is the time period of FeS_B formation (trace C). The FeS_A species is not observed in this scenario (trace A) (adapted from (64)).

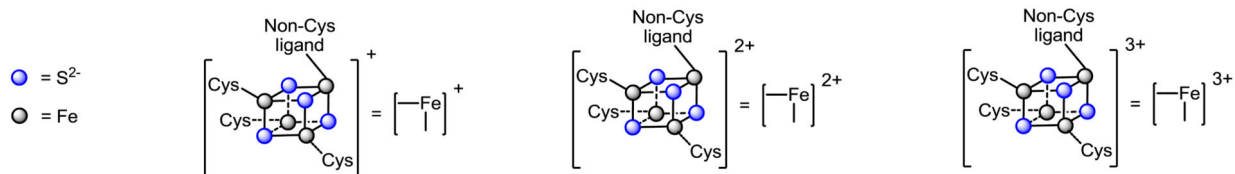
Author Manuscript

Author Manuscript

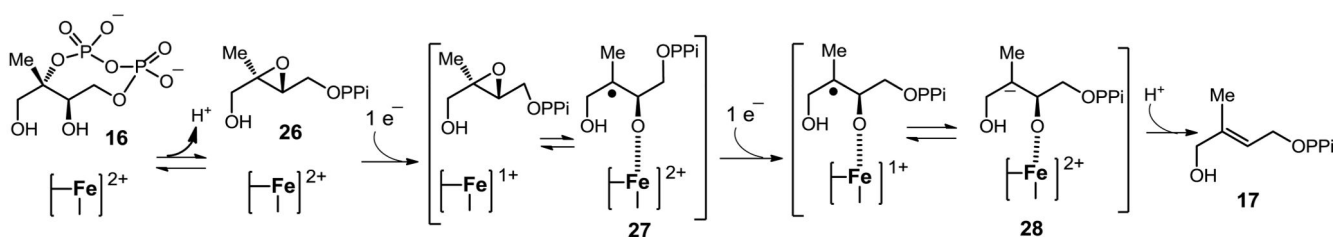
Author Manuscript

Author Manuscript

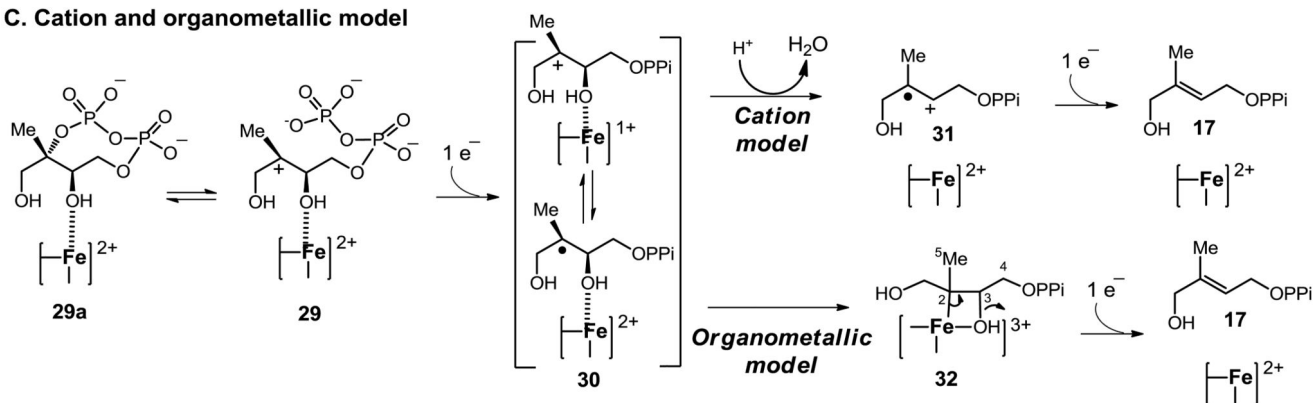
A. Symbols used in describing the mechanistic models



B. Epoxide model



C. Cation and organometallic model



D. IspG-catalyzed reactions

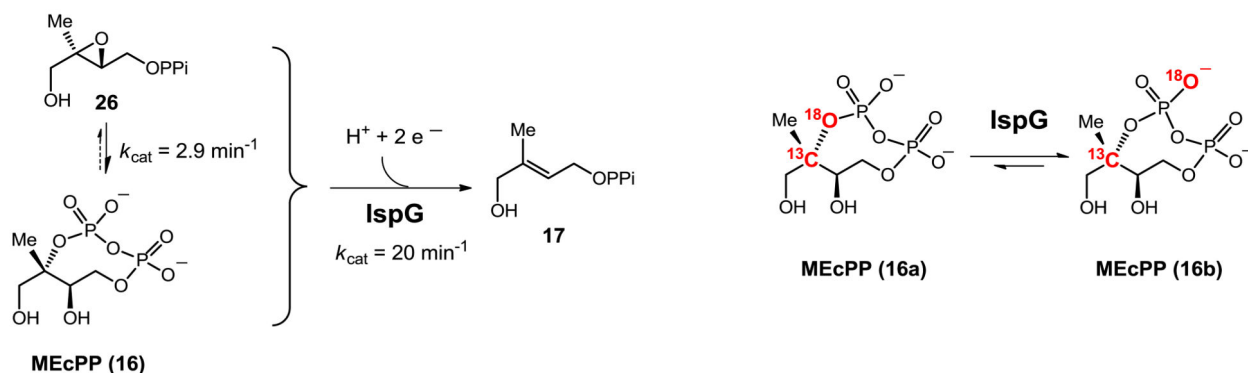


Figure 4.

Proposed IspG mechanistic models. **A.** Symbols used to represent the iron-sulfur clusters. **B.** The epoxide model. According to this model, the epoxide (**26**) is an obligate intermediate of the MEcPP reductive dehydration. Once the epoxide (**26**) is formed, two sequential one-electron reductions mediated by the iron-sulfur cluster lead to HMBPP (**17**) formation. The Lewis acidity of the [4Fe-4S] cluster might also facilitate the dehydration process (**28** \rightarrow **17** conversion). **C.** Cation and organometallic models. In these two models, the formation of a cation intermediate (**29**) by the C₂ C-O cleavage is the first step. Once the cation

intermediate (**29**) is formed, subsequent reductive dehydration can follow either the cation model via a radical cation intermediate (**31**) or the organometallic model via the organometallic intermediate (**32**). **D.** IspG-catalyzed reactions. IspG can catalyze both the reductive deoxygenation of **26** and the reductive dehydration of **16** to **17**. However, in the absence of reductants, IspG catalyzes an irreversible **26** → **16** conversion. MEcPP (**16**) itself is stable for weeks at room temperature, while in the presence of holo-IspG and the absence of reductants, a positional isotopic exchange (**16a**↔**16b**) is observed.

Author Manuscript

Author Manuscript

Author Manuscript

Author Manuscript

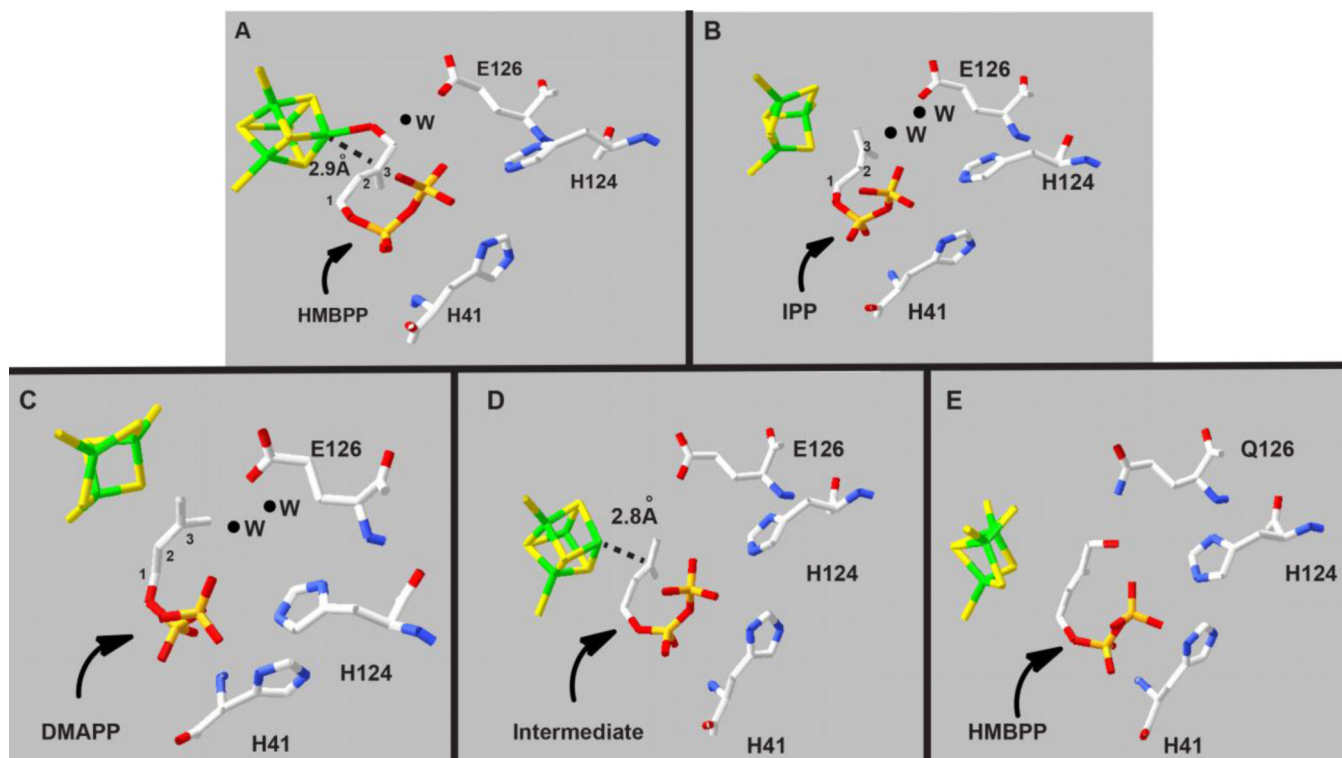
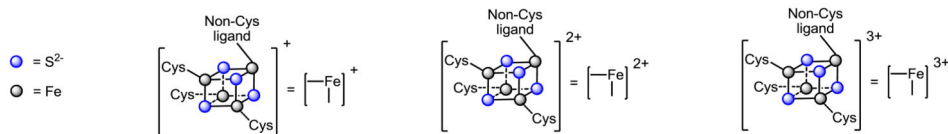
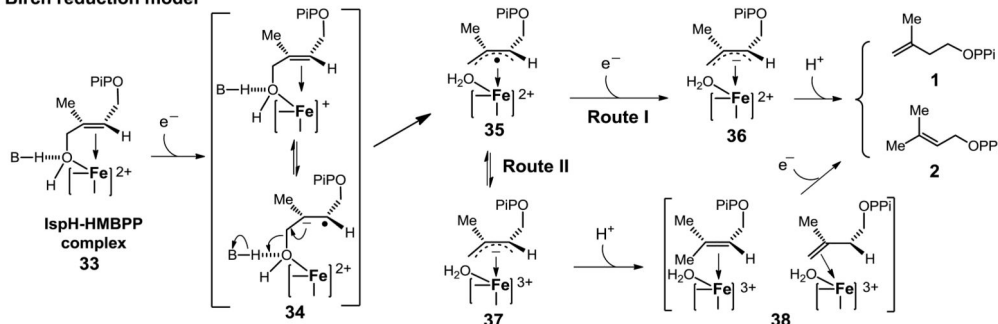


Figure 5. Representative IspH structures revealing IspH structural flexibility. **A.** The crystal structure of IspH-HMBPP complex at 1.7 Å resolution. This structure reveals a few important features, including the direct coordination between the HMBPP C₄-OH to the [4Fe-4S] cluster unique iron site and a short distance (2.8 – 3.0 Å) between the HMBPP olefinic functional group (C₂ and C₃ carbons) and the [4Fe-4S] cluster unique iron site. **B.** The IspH-IPP complex. In this structure, the active site has two water molecules. In addition, IPP C₁ carbon adopts a conformation distinct from that in the IspH-HMBPP complex in Figure 5A. **C.** The IspH-DMAPP complex. This structure also shows two water molecules in the active site. **D.** On-beam conversion of the IspH-HMBPP complex. Relative to the structure in Figure 5A, the HMBPP C₄-OH is gone. In addition, the distance between the HMBPP olefinic functional group (C₂ and C₃ carbons) to [4Fe-4S] cluster unique iron site decreases to 2.6 – 2.8 Å. It is not yet known whether this is the product complex or an intermediate. **E.** The IspH E126Q mutant and HMBPP complex. Relative to the structure in Figure 5A, the HMBPP C₄-OH rotates to the other side of HMBPP olefinic functional group (C₂ and C₃ carbons) and forms an internal hydrogen bond with its terminal phosphate. In this complex, there is no water in the active site.

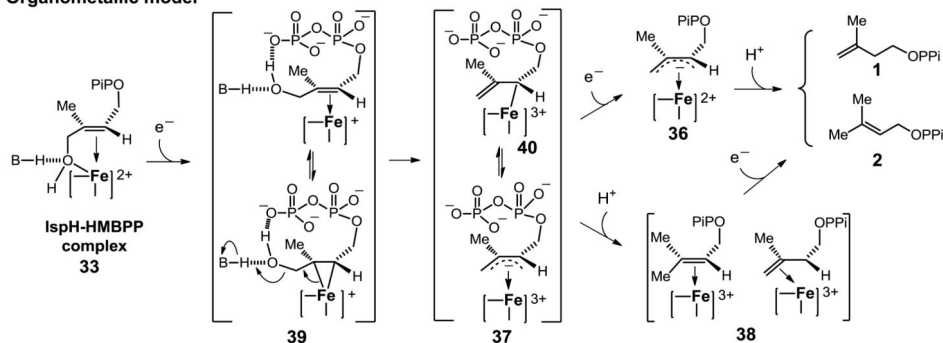
A. Symbols used in describing the mechanistic models



B. Birch reduction model



C. Organometallic model



D. Two potential binding modes for mechanistic probe 43.

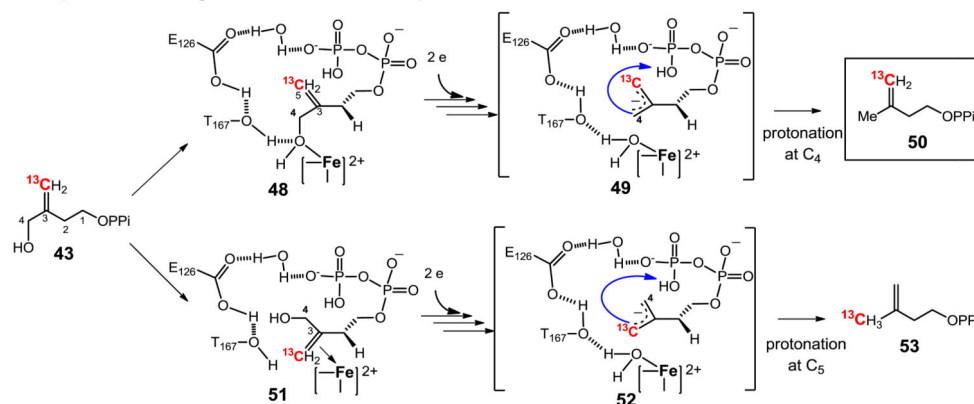


Figure 6.

Proposed IspH mechanistic models. The formation of the IspH-HMBPP complex (**33**) is the only well-established step and steps after **33** are highly debated (Birch reduction model vs. Organometallic model). **A.** Symbols used to represent the iron-sulfur clusters. **B.** Birch reduction model. In this model, the IspH iron-sulfur cluster has two roles: mediating two step-wise one-electron reduction steps (**33** \rightarrow **34** and **35** \rightarrow **36**) and serving as the Lewis acid to facilitate C₄-dehydration (**34** \rightarrow **35**). **C.** Organometallic model. In this model, there are also two unique features: the rotation of the HMBPP C₄-OH group away from the

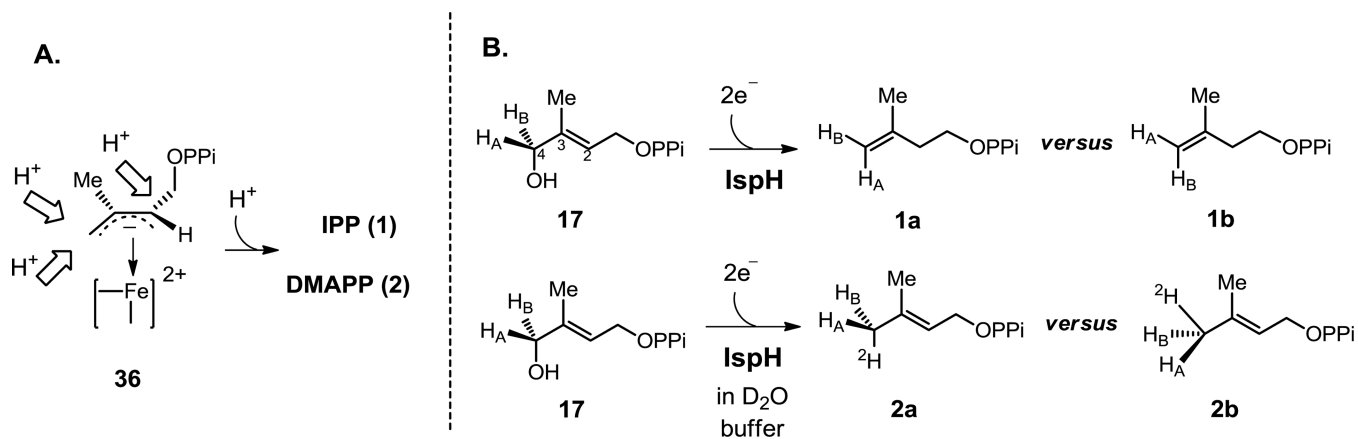
[4Fe-4S] cluster to form an internal H-bond (**39**) and an iron-sulfur cluster mediated one-step two-electron reduction (**39** → **40**). **D**. Two possible binding modes for mechanistic probe **43** (**48** vs. **51**).

Author Manuscript

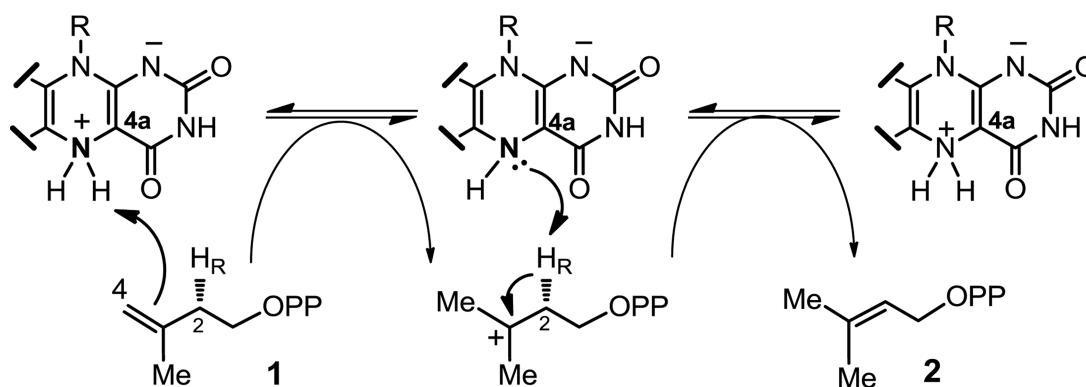
Author Manuscript

Author Manuscript

Author Manuscript



A. IDI-2 mechanistic models



B. Selected examples of IDI-2 mechanistic probes

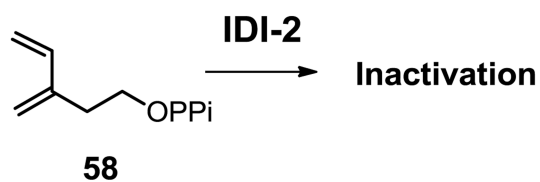
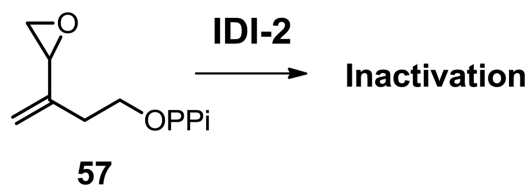
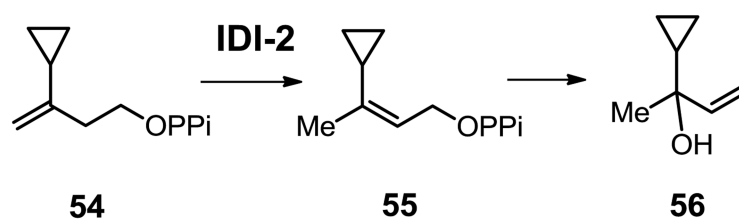


Figure 8. IDI-2 mechanistic model and selected mechanistic probes. **A.** IDI-2 mechanistic model. The flavin cofactor functions as both acid and base to complete the catalytic cycle. **B.** A few selected IDI-2 mechanistic probes.

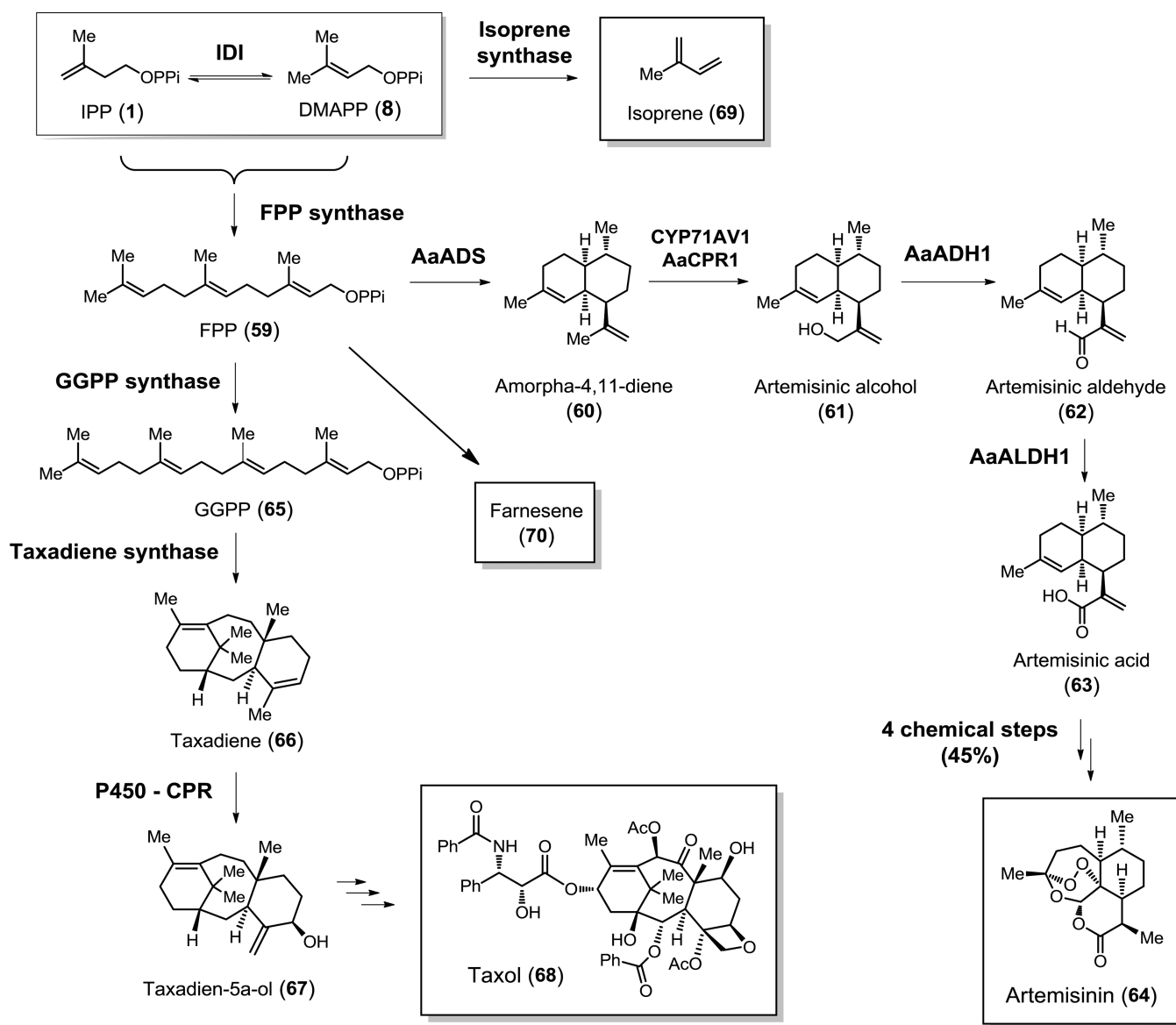
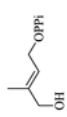
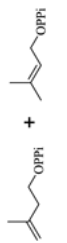
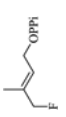
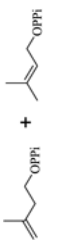
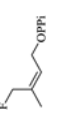

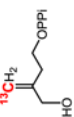
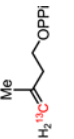
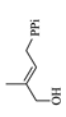
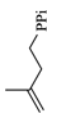
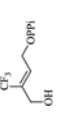

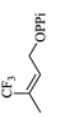
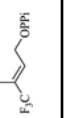


Figure 9.

High level microbial production of artemisinin precursors, isoprene and taxol precursors through metabolic engineering of either MVA or MEP pathway. Isoprenoid production through metabolic engineering normally involves two parts: 1) the production of a common intermediate FPP (59) by FPP synthase from IPP (1) and DMAPP (2) supplied by either the MEP or the MVA pathway (Figure 1); 2) After FPP, by introducing enzymes specific to a product of interest (e.g., Artemisinin (64), Taxol (68), or Isoprene (69)), *E. coli* or yeast can then be tailored by introducing the corresponding genes to produce a specific product.

Table I

Various mechanistic probes used to study IspH catalysis.

Probes	Compound number	k_{cat} (min^{-1})	K_m (μM)	k_{cat}/K_m ($\mu\text{M}^{-1}\text{min}^{-1}$)	Product	Product ratio
	17	604 ± 17	19.7 ± 2.4	30.6		IPP: DMAPP ~5 : 1
	41	27.7 ± 2.2	104 ± 31	0.27		IPP: DMAPP ~7 : 1
	42	8.4 ± 1.9	489 ± 170	0.02		Only IPP
	43	484 ± 1.5	694 ± 74	0.68		Only IPP
	44	0.55	3950	2.52×10^{-4} (notes)		Only IPP analog
	45	91.6 ± 2.2	447 ± 32	0.21		Only IPP analog
	46	No detectable activity	No detectable activity			
	47	No detectable activity	No detectable activity			